Design and Implementation of a High Speed Cable-Based Planar Parrallel Mechanism

by

Edmon Hok-Man Chan

A thesis

presented to the University of Waterloo

in ful...llment of the

thesis requirement for the degree of

Masters of Applied Science

in

Mechanical Engineering

Waterloo, Ontario, 2005

I hereby declare that I am the sole author of this thesis.
I authorize the University of Waterloo to lend this thesis to other institutions or individuals for the purpose of scholarly research.

Edmon Hok-Man Chan

I authorize the University of Waterloo to reproduce this thesis by photocopying or other means, in total or in part, at the request of other institutions or individuals for the purpose of scholarly research.

Edmon Hok-Man Chan

The University of Waterloo requires the signatures of all persons using or photocopying this thesis. Please sign below, and give address and date.

Acknowledgements

Add your Acknowledgement here

Abstract

Add your Abstract here.

Contents

List of Tables

List of Figures

Chapter 1

Introduction

Industry always thrives for a higher quality and more economical process. Robotic automation has been a primary driving force for improving on modern manufacturing process. A fast and accurate pick-and-place operation is a desired robotic application for many industrial sectors. Typical pick–and-place applications such as packaging, assembly, and part sorting require manipulation of an object on a ‡at surface. It is a common practice to stack multiple planar manipulators together while using a conveyor to feed a matrix of objects in the direction normal to the manipulator workspace. This approach usually saves precious manufacturing space in an industrial environment. In this work, a new type of 2D cable-based parallel manipulator that is intended for high speed pick-and-place application for light object is introduced

The primary requirements for pick-and-place operations are high accuracy, high speeds, and high repeatability. High accuracy can only be attained if the robot construction is sti¤ enough to suppress deformation; high speed, on the other hand is limited by the actuator power and the robot moving inertia. Since high sti¤ness usually comes at the expense of increasing inertia, a designer must …nd the right balance for their particular solution. The most common industrial robotic manipulators nowadays are Cartesian table and Gantry manipulators. These types of con…guration append independent motions from one link to another in a serial fashion, hence they are classi…ed into the serial robot family. Due to the natural of design, the robot actuator, or at least the power chain that is connected to the actuator must move with the manipulator. As a result, serial robot trends to have a large moving inertia to payload ratio regardless of the size of the actuator.

A new type of robotic design, called parallel mechanism has emerged from recent robot development. This type of robot is constructed by attaching multiple independently actuated kinematics chains to a mobile platform concurrently. Since the kinematics chains do not stack from one to another, any force that is applied to the mobile platform would be distributed amongst multiple linkages. This e¤ectively increases the sti¤ness of the robot structure. Moreover, the actuators of each chain can be …xed on to a base, and they do not become part of the moving inertia. These two properties lead to an inherent advantage on sti¤ness and inertia over their serial counterpart. With the leading edge on sti¤ness and inertia, parallel mechanisms have quickly found their way into many high speed pick and place applications. Among which, the Delta con…guration is arguably the most successful design in the last decade. Most of the recent parallel robot designs can achieve 150 cycles per minutes [1].

If the underlying principal of the success in high speed pick-and-place robot is light and sti¤, there must be other method to improve on the robot performance by further reduction in moving inertia without compromising too much on structural sti¤ness. This thesis document, design and implementation of a high speed cable-based planar parallel mechanism attempts to improve the sti¤ness to inertia ratio by replacing rigid linkages of the kinematics chain with ‡exible cables. Mechanical cable, which is virtually massless, processes a relatively high mechanical strength under tension. The fundamental principle of this design approach is to replace the heavy linkages with cable. An additional advantage of using cables is that they can replace some revolute joints, which are relative costly and unreliable due to the limited component life expectancy. Furthermore, there are several design issues that must be addressed when using cables in a mechanism.

The layout of this thesis is as follows: Chapter 2 presents the literature review of some parallel mechanism and design consideration that are speci…c to cable-based mechanism. Chapter 3 introduces the conceptual design and the theoretical development for this new class of cable based robot. It also addresses the primarily design requirements that satisfy the design constraints. Chapter 4 discusses the details design strategy and optimization process. It also o¤ers a systematic methodology that requires only the inverse kinematics equations for the development of this class of robot. Chapter 5 provides a more detailed design implementation of

[1] for more information, refer to http://www.abb.com/robotics

two robots that uses this design. The inverse kinematics equations of both robots are developed along with the design procedure. Chapter 6 then goes in the kinematics calibration and the experimental evaluation on a prototype that is build in the University of Waterloo. Chapter 7 summarizes the conclusions of the work and highlights future research works.

Chapter 2

Literature Review

2.1 Introduction of Parallel Manipulator

This thesis work focuses on two aspect - Parallel Mechanism and Cable Based Manipulator. It is appropriate to introduce the parallel mechanism in this chapter. Parallel Mechanism, or sometimes referred as closed chain mechanism is a relatively new concept in industry. However, their actual theoretical work can be dated centuries ago [1]. Tsai, a pioneer in recent parallel manipulator developments has once compared di¤erent type of parallel mechanism, and describes them to be "a mechanism that is typically consists of a moving platform that is connected to a …xed base by several limbs" [14]. For many parallel manipulators, all of the limbs (kinematics chain) are of the same kind and the orientation degree of freedom is usually coupled with the translation degree of freedom.

Early parallel mechanisms are usually targeted for 6 degrees of freedom. The simplest implementation is Gough Platform designed by Gough and Whitehall in 1947 [11]. In that design, the moving platform is actuated by 6 linear actuators that connects the base and the moving platform through spherical joints as shown in Figure 2-1. This con…guration have been used in ‡ight simulator [27] and Ingeroll's milling machine [13]. One of the most successful implementation of parallel mechanism is the Delta invented by Clavel in 1990s [8]. In Delta, the moving platform is actuated by three pairs of synchronized elementary chain that are driven

[1] Interested reader are refered to http://www.parallemic.org/Reviews/Review007.html for more details

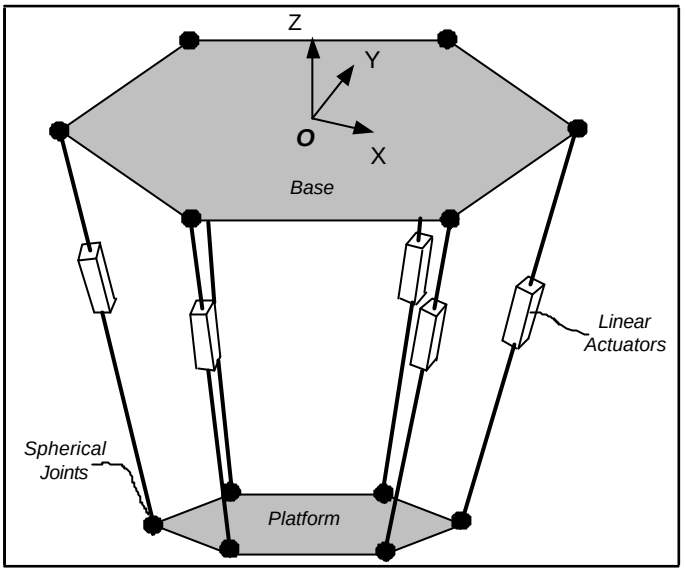

Figure 2-1: Schematic of Stewart platform

independent by a rotary actuators as illustrated in 2-2. This con…guration eliminate any rotational degree of freedom and hence produces a three translational DOFs manipulator.

Ever since Clavel published his invention, a signi…cant amount of research activities has been conducted to improve the design of Delta and many other similar parallel con…gurations [26], [19], [18], [5]. Some of the research work has been directed towards a 2 translational degrees of freedom (DOF) version of the parallel mechanism. Ghorbel developed Rice Planar Delta Robot (RPDR) in the 90's to demonstrate various control and analysis techniques for parallel robots [10]. RPDR is kinematically similar to Delta as shown in Figure 2-3, and it is originally designed for experimental purpose. The orientational degree of freedom in RPDR is coupled with the translational degree of freedom which make limits its uses. This shortcoming has been overcame by another design due to Huang et al [12]. In that design, a pairs of parallel link is used to connects the moving platform to the …rst link, much like the original Delta design. This planar delta has only translational degree of freedom was intended for high speed pick and place operations.

From the development points of view, some of these researches introduce analytical methods to analyses the complex forward kinematics of parallel robots [6] [24]; others address more

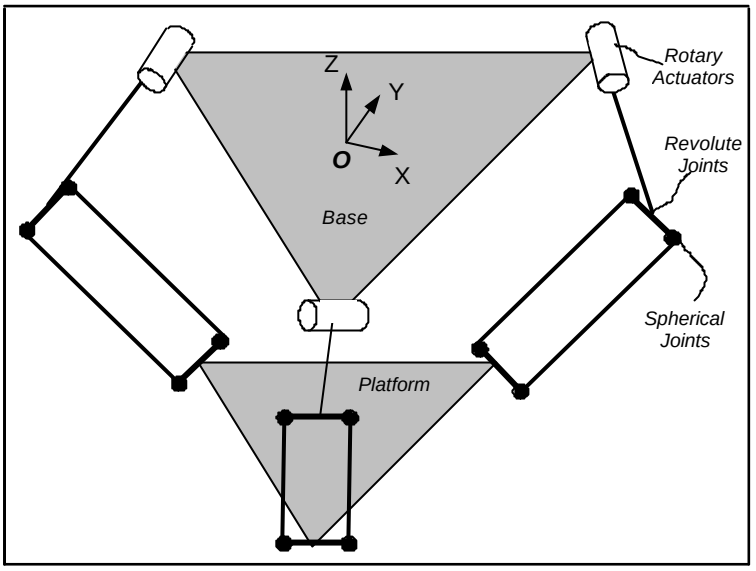

Figure 2-2: Schematic of Delta

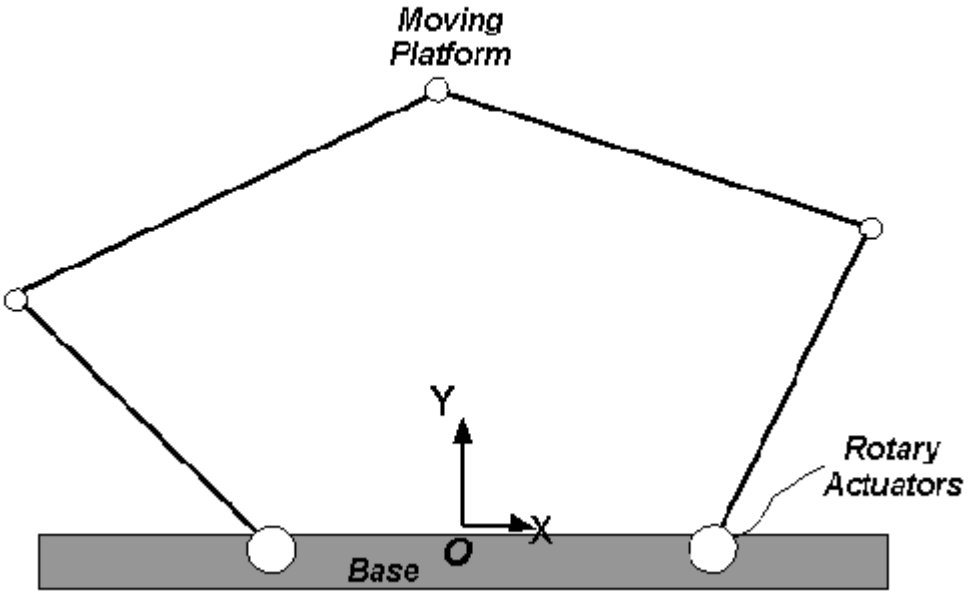

Figure 2-3: Schematic of Rice Planar Delta Robot

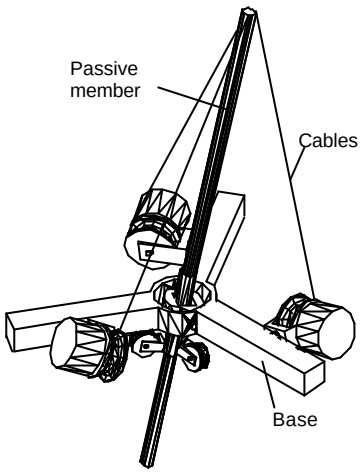

Figure 2-4: Picturial View of Landsberger robot

subtle issues like inherent problems such as internal singular con…guration [25]. However, these analytical tools are subjected to certain speci…c conditions, and there is still no universal systematic method to analyze parallel mechanism.

2.2 Cable based Mechanism

While there are already signi…cant amount of parallel manipulators design in recent literatures, one class of parallel mechanism that uses cable in its kinematics chain is of particular interest in this work. A cable-based parallel manipulator usually means a lower moving inertia and lower manufacturing cost when compared to their rigid link counterpart. Moreover, the ‡exibility of a cable allows them to replace some mechanical joint and same more robot space in some design. However, a cable based robot does not come without any drawback. Cable is only useful if it can held under tension, and some of the research work were directed towards the tensioning of cable in cable-based robot. Ming and Higuchi, performed earlier study on the tension distribution in cable-based manipulators for high DOF cable based-manipulators [2] in 1996, Tadokoro et all, designed cable wire robots using 8 cables (with 2 of redundant cables) for a 6 DOFs of motion[28]

Early cable-based parallel robots were designed mainly for speed enhancement Landsberger developed a 3 DOFs cable-based manipulator that is somewhat an extension to the Stewart-Gough platform. In Landsberger's design, three cables are attached to a telescopic compression member as shown in Figure 2-4. The lengths of the cables are independently controlled by winches to position the end-e¤ector in 3D space [20]. Early implementation of the Landsberger robot was capable of reaching a speed of 3.5m/s.

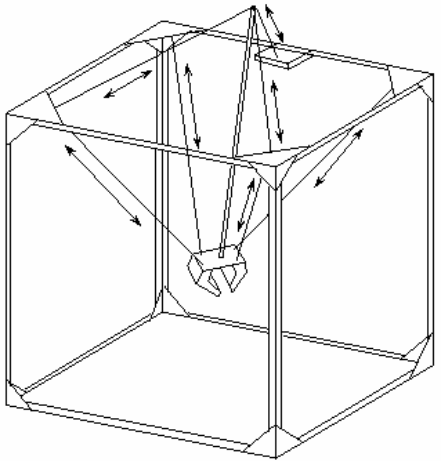

Figure 2-5: Schematic of Falcon

Another cable-based manipulator design that features a high degrees of freedom and a large workspace is Falcon, developed in mid 90s. Falcon was designed for a positioning application [15]. There are 7 cables in the design with one of them to be a redundant kinematics chain that induce the tension for the other cables as shown in Figure 2-5. Due to the light inertia design, Falcon is capable of achieving 43g of acceleration and a peak velocity of 13m/s. This is one of the class cable-based manipulators that demonstrates high mobility and fast dynamic characteristic.

Over the pass couple decades, Cable-based manipulators have proven to be suitable choice of design approach for high speed machineries. This thesis work would be focused on the development of a planar cable-based parallel mechanism that can achieve a even higher dynamic response for industrial applications.

Chapter 3

Robot Design Overview

The essence of a high speed manipulator design is to reduce the moving inertia while maintaining the sti¤ness. Sti¤ness can be increased if the disturbance forces are transmitted through multiple paths. Parallel mechanisms apply this principal e¤ectively, which produces an inherent advantage on sti¤ness and can be constructed with lighter components. In order to further reduce the moving inertia, this work proposes to construct some of the linkage with cable wire. This method can be applied to most common parallel robot con…guration with simple kinematics train. However, there are a few issues that need to be addressed to avoid mechanical failure. This chapter investigates the problems concerning a cable construction.

3.1 Conceptual Design

The proposed cable-based design is a planar manipulator. It consists of a …xed base, a pair of parallel cables, a third cable, a telescopic spine (central pose), and an end-e¤ector as illustrated in Figure 3-1. This design is focused on the mobile end of the manipulator where a pick-and-place tool is to be mounted on the moving platform.

The spine is attached to the end-e¤ector by a revolute joint with its pivoting axis perpendicular to the plane of action. The objective of the spine is to induce a tensile force on the cables. The paired cables are separated by a …xed distance. When they are held under tension, these cables form a parallelogram. Due to the geometric constraint on this parallelogram, the

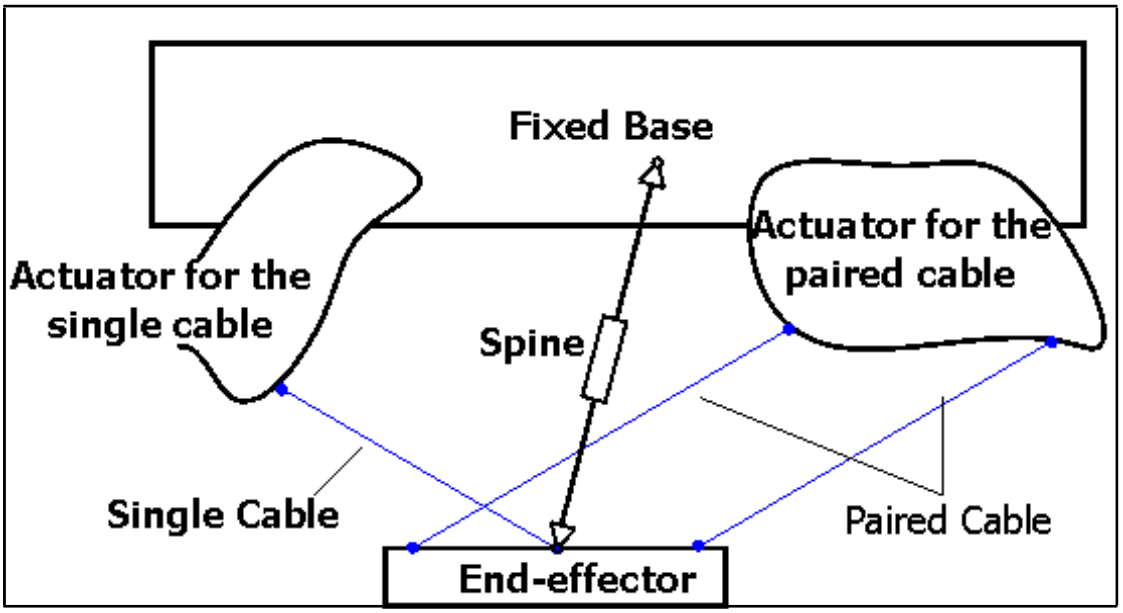

Figure 3-1: A schematic of proposed cable based 2DOF planar mechanism

orientation degree of freedom is controlled. Here this pair of parallel cables is de…ned as a parallel cable joint.

De…nition 1 A parallel cable joint is a joint made of two parallel cables attached to a rigid element E. The centerline direction of the cables is OO¤ and can vary in time see …gure 3-2. The cables are assumed to be held under tension (positive T_1 and T_2).

There are two distinct types of component in the propose robot design. A natural way to classify them into assembly is based on their function:

De…nition 2 The upper robot assembly is the portion of the manipulator that is responsible for the kinematics characteristic. This portion includes the base, and the drive train.

De…nition 3 The lower robot assembly is the portion of the manipulator that is responsible for manipulating the end-e¤ector. The large amount of motion makes it the dominant contributor to the overall dynamic characteristic. This portion is composed of the end-e¤ector and the spine.

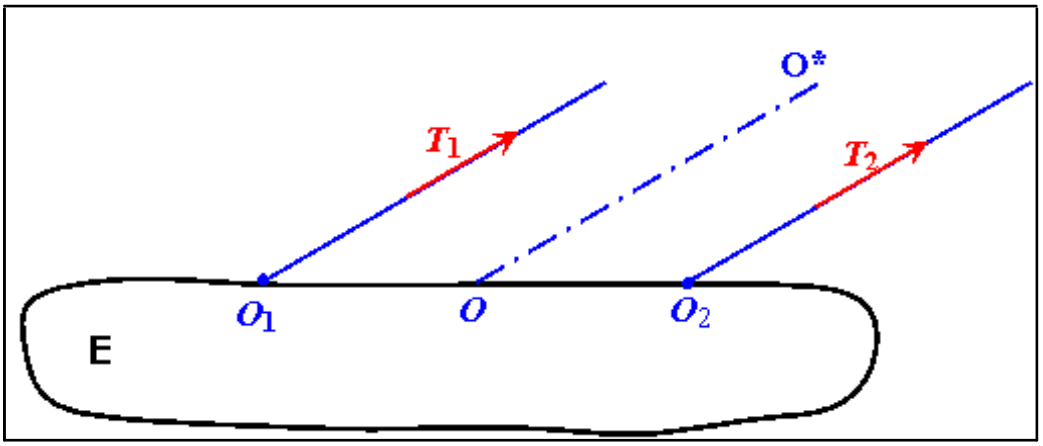

Figure 3-2: Parallel Cable Joint

3.2 Theoretical Development of 2D Cable based robot

A solid linkage can withstand tension, compression and bending. Depending on the length, solid linkages usually have a low mass to compressive strength ratio. Similarly, bending sti¤ness is usually poor for slender linkages. Therefore, it is highly bene…cial to operate linkages under tension only. Under the assumption that a mechanical component operates under tension, there is little di¤erence whether that component is a piece of cable or a rigid solid linkage. As a result, in cable-based manipulators, there is an element to provide tension to the cables. This element is called spine and can be another cable, a pneumatic cylinder or a spring. Before investigating the detail aspect of the necessary operation conditions for these cable-based robots, it is appropriate discuss a few concepts that allow a cable robot to behave as if it were constructed with rigid elements.

De…nition 4 Rigid pose: A cable-based manipulator is considered to be in a rigid pose, if the manipulator is not at a singular pose and all of the cables are held in tension under a given set of external loads. Therefore, a cable robot that is in a rigid pose is considered as a structure.

De…nition 5 Tensionability: A non-singular pose is tensionable if and only if for any arbitrary external load, there exists a …nite spine force to make the manipulator rigid. Tensionability, the ability to apply tension to a mechanical component (in this case, the cable) is a

necessarily condition to maintain a cable-based manipulator in a rigid pose regardless of any other external load.

Since a useful manipulator must be able to guarantee its rigidity everywhere within the workspace, it is necessary to seek some insight to tensionability of a manipulator. In this chapter, a design strategy that always satis…es the tensionability criterion of a 2D cable-based manipulator will be discussed.

When a manipulator is in a rigid pose, it does not translate nor rotate. Assuming the cable axes are independent and the two of the cables form a parallel cable joint, the manipulator will not be in a singular position. In order for a manipulator to be considered at a rigid pose, the tensionability is the only remaining condition that needs to verify. Since the cable tensions are profoundly dependent on the spine force, the very …rst condition that shall be examined is the su¢cient spine placement to ensure tensionability. The investigation begins with a simple non-translating end-e¤ector setup. That con…guration leads to necessary spine position to produce a tensionable con…guration under no external load. The analysis is then extended for the tensionability condition under which the manipulator is tensionable for any …nite load (and torque) and a generalized end-e¤ector con…guration.

3.2.1 Tensionable Con…guration

A) Zero Translational Requirement (with a speci…c external load)

Suppose two cables are attached to point O of the end-e¤ector under an external load P as seen in Figure 3-3. The end-e¤ector will not translate if the tension in cables T_A and T_B can balance the external load P. This in fact indicates that if the manipulator is tensionable, there exists a set of positive T_A and T_B to balance the external force P. If P lies between the cables bases, (OL_1^0 and OL_2^0), it can be projected onto the bases axis with a positive component. As a result, there exists a set of positive cable tension to cancel out the component of force resolved in each of the cable axis. Therefore, the manipulator is tensionable as long as P lies inside the positively linearly dependent space spanned by T_A and T_B. A corollary is that the negation of the force vector, P that lies between the cable axes must also lie inside the positively linearly dependent space spanned from T_A and T_B. Also note that an increasing P monotonically

increases T_A and T_B as the magnitude of the force component increases.

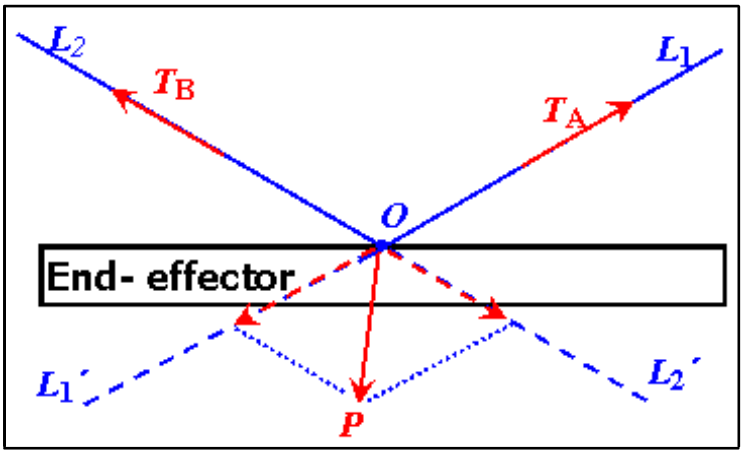

Figure 3-3: Zero Translation platform

B) Translational and Rotational Requirement (In the absence of external load and torque)

Suppose a parallel cable joint is attached to an end-e¤ector such that its centerline coincided with the third cable and a spine as shown in Figure 3-4. The point where all components are coincided is de…ned to be point O. The assembly is completely in a rigid pose (all cables are in tension, zero translation and zero rotation) i¤ the spine axes, OL_3 is between the cable axes, OL_1 and OL_2 and it exerts a compressive force F_C onto the rigid body at point O.

This con…guration is an extension to Case A. Let $T_A = T_{A1} + T_{A2}$, there exists positive T_A and T_B for any value of F_C that constrains the translational DOF as shown in Case A. To satisfy the torque equilibrium condition, $\sum_P M = 0$ (in the absence of any external torque), T_{A1} and T_{A2} are selected to be:

$$T_{A1} = T_{A2} = \frac{T_A}{2} \tag{3.1}$$

C) Zero Translational Requirement with any arbitrary external load

Suppose two cables with axes OL_1 and OL_2, and a spine with axis OL_3 orientated between the cable axes are connected to the end-e¤ector as shown in Figure 3-5. This con…guration can

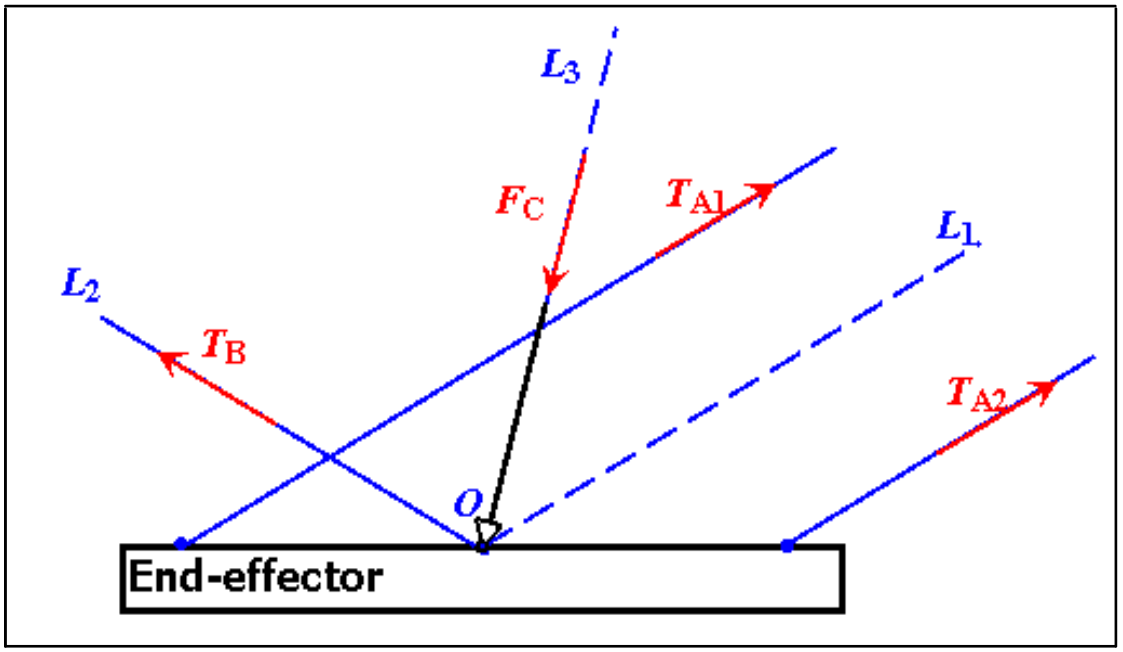

Figure 3-4: Zero translational and rotational end e¤ector under no load

balance any …nite external force P, in any arbitrary direction and therefore is in a tensionable con…guration.

Although this result can be directly observed if one realizes the axes OL_1, OL_2, and OL_3 form a positively linearly dependent basis on a 2D plane, it is worthwhile to quantitatively analyze the problem. The external force can be resolved into an orthogonal basis that is aligned to axe OL_3. The component that is parallel to the OL_3 is P^t, and the component that is normal to OL_3 is P^n. Using the superposition of forces, the system is in force equilibrium (translational rigidity) if both components of the external force can be balanced by the applied load F_C, T_A, and T_B, all with a positive magnitude (tensionable).

The tangential component, P^t produces a tensionable con…guration if it is positive (pointing away from the cables) as explained in Case A. If the force component is negative, a contribution of F_C is needed to force the sum of the force to become positive. Therefore, the tangential component always forms a tensionable con…guration.

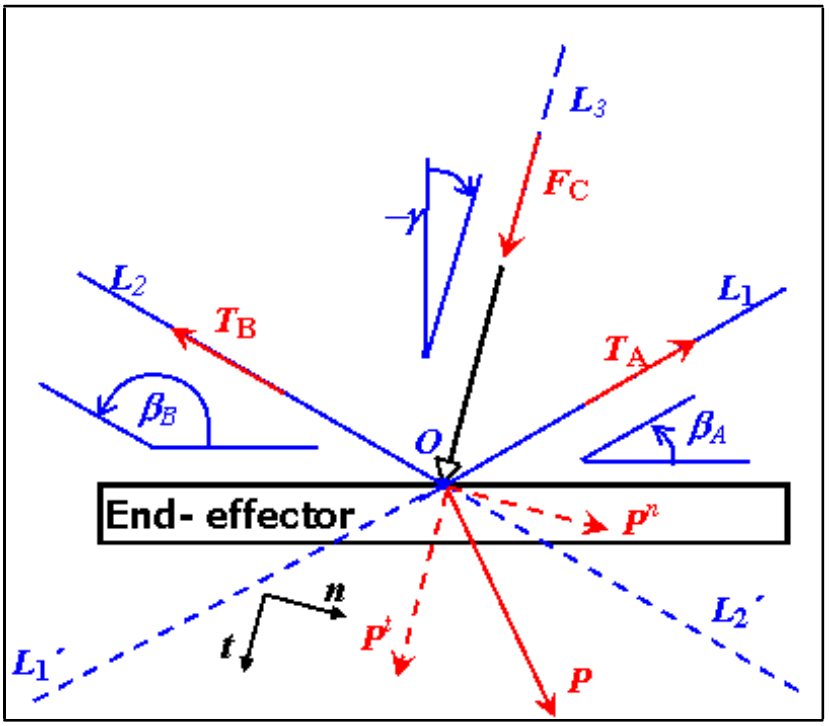

Figure 3-5: Zero Translational end e¤ector under any arbitrary load

As for the normal component, P^n, it can either lie between OL_1^0 and OL_2^0, or outside the OL_1^0-OL_2^0 envelope. If it were the former case, the situation is identical to Case A and the system is tensionable. If it were the later case, a positive component of F_C is needed to bring P^n onto OL_2^0 for a positive P^n, and onto OL_1^0 for a negative P^n (see Figure 3-5). Therefore, the normal component also forms a tensionable con…guration.

Note that at this point it is possible to compute the cable tensions. Let F_C^0 be the summation of F_C and P^t, it can be shown through geometry and force equilibrium that the cable tension T_A and T_B can be computed by a set of linear equations. The force equilibrium shows:

$$\sum F_x = T_A \cos(\theta_A) + T_B \cos(\theta_b) + F_C^0 \sin(\eta) + P^n \cos(\eta) = 0$$

$$\sum F_y = T_A \sin(\theta_A) + T_B \sin(\theta_b) - F_C^0 \cos(\eta) + P^n \sin(\eta) = 0$$

In matrix form:

$$\begin{bmatrix} \cos(\theta_A) & \cos(\theta_B) \\ \sin(\theta_A) & -\sin(\theta_B) \end{bmatrix} \begin{Bmatrix} T_A \\ T_B \end{Bmatrix} = \begin{bmatrix} -\sin(\eta) & -\cos(\eta) \\ \cos(\eta) & -\sin(\eta) \end{bmatrix} \begin{Bmatrix} F_C^0 \\ P^n \end{Bmatrix}$$

Rearrange and simplify the equilibrium equations using trigonometric identities produce:

$$\begin{Bmatrix} T_A \\ T_B \end{Bmatrix} = \frac{1}{\sin(\beta_B - \beta_A)} \begin{bmatrix} -\cos(\theta - \beta_B) & \sin(\theta - \beta_B) \\ \cos(\theta - \beta_A) & -\sin(\theta - \beta_A) \end{bmatrix} \begin{Bmatrix} F_C^0 \\ P^n \end{Bmatrix} \tag{3.2}$$

D) Zero Translational and Rotational Requirement with arbitrary load

The cable robot in Figure 3-6 is shown to be in a rigid con…guration for any external force, P and torque, M with a …nite amount of spine force F_C.

The end-e¤ector forms a rigid con…guration if there exists a set of positive T_{A1}, T_{A2}, and T_B, and F_C for any given applied loads that satis…es the force equilibrium equations:

$$\begin{aligned} \sum F &= 0 \\ \sum M_O &= 0 \end{aligned}$$

Suppose the tension forces TA_1 and TA_2 are replaced with an equivalent force T_A and a torque M_A at point O. Note that T_A is also aligned to the cable axis A. By applying the superposition principle on the translational system (i.e. ignoring the torque), it can be observed that the translational sub-system is identical to Case C. Therefore there exists a spine force, F_C that induces a tensile force on the cables.

As for the rotational system, consider the parallel cable joint in Figure 3-7. The system is tensionable for a …nite amount of applied torque, M. The torque capacity of a parallel cable joint - the amount of applied torque that a parallel cable joint can balance is depended on the amount of the total tension on both cables. The equations of the force / torque equilibrium about point O are:

$$\sum F_y = 0 : T_A = T_{A1} + T_{A2} \tag{3.3}$$

$$\sum M_O = 0 : M = T_{A1} d \sin(\beta_A) - T_{A2} d \sin(\beta_A) \tag{3.4}$$

If both of T_{A1} and T_{A2} are positive, and knowing neither T_{A1} nor T_{A2} is bigger than T_A, it can be concluded that the maximum torque that can be applied to the parallel cable joint

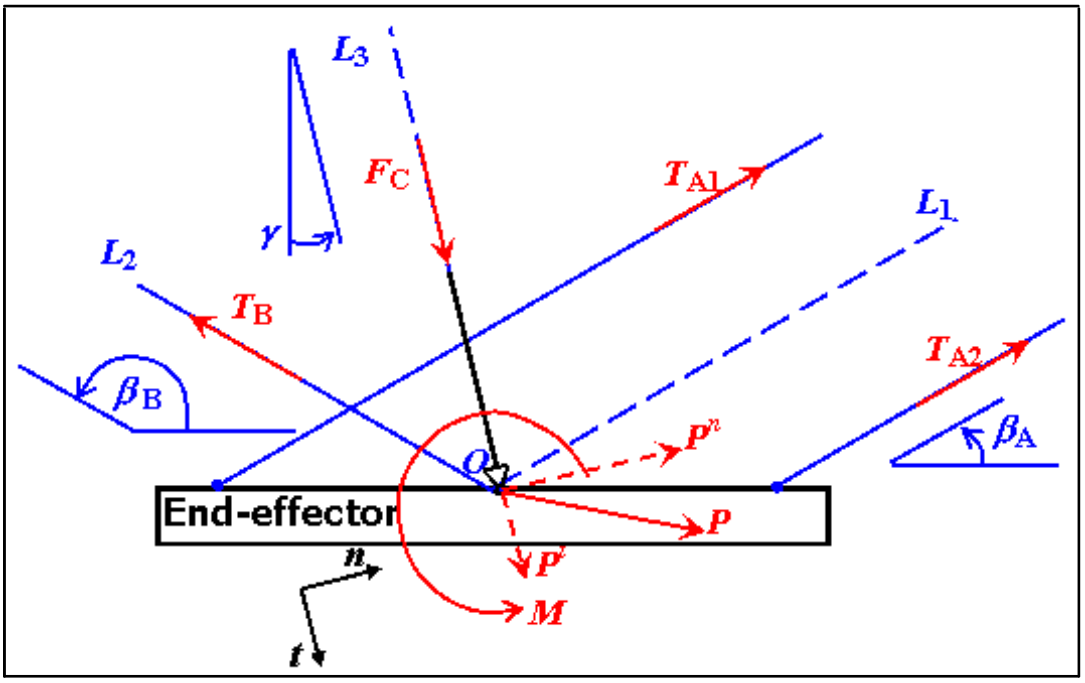

Figure 3-6: Zero Translational and Rotational end e¤ector under arbitrary load and moment

without losing the cable tension must satisfy the following inequality:

$$¡ T_A d \sin(\bar{}_A) \cdot M \cdot T_A d \sin(\bar{}_A) \tag{3.5}$$

Note that the torque capacity is heavily depended on T_A which in turns holds a linear relationship with F_C from Case B. Therefore, an increase in F_C would generally result in a larger torque capacity on the parallel cable joint. It can be concluded that there exists a …nite spine force to generate a large enough torque capacity to form a rigid pose for the rotational system. Therefore the entire system is tensionable.

It is necessary to compute the minimum spine force and the cable tension quantitatively in the design process. Solving Equations (3.3) and (3.4) simultaneously produces:

$$\begin{Bmatrix} T_{A1} \\ T_{A2} \\ T_B \end{Bmatrix} = \begin{bmatrix} 0{:}5 & 0 & \frac{1}{2d\sin(\bar{}_A)} \\ 0 & 0{:}5 & ¡\frac{1}{2d\sin(\bar{}_A)} \\ 0 & 1 & 0 \end{bmatrix} \begin{Bmatrix} T_A \\ T_B \\ M \end{Bmatrix} \tag{3.6}$$

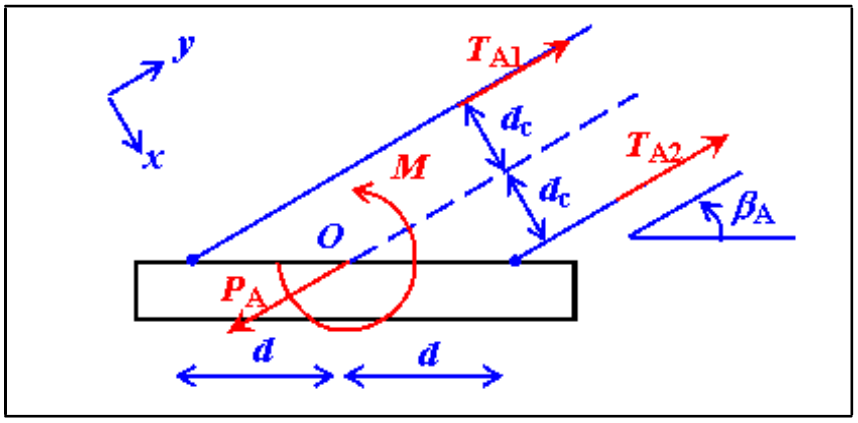

Figure 3-7: Torque capacity of a parallel cable joint

Here, two set of forces that are important to the dynamic behaviour of the robot should be de…ned:

$$fTg = \begin{Bmatrix} T_{A1} \\ T_{A2} \\ T_B \end{Bmatrix} \tag{3.7}$$

$$fLg = \begin{Bmatrix} F_C^{\emptyset} \\ P^n \\ M \end{Bmatrix} \tag{3.8}$$

The cable tension vector (3:7), which consists of the tension of the individual cable, and the load vector (3:8), which is a set of external load and moment typically due to the inertia force from to a moving body.

Appending the applied moment M to Equation (3:2) produces a mapping function that involves L:

$$\begin{Bmatrix} T_A \\ T_B \\ M \end{Bmatrix} = \begin{bmatrix} \frac{i\cos(° i \bar{} _B)}{\sin(\bar{} _B i \bar{} _A)} & \frac{\sin(° i \bar{} _B)}{\sin(\bar{} _B i \bar{} _A)} & 0 \\ \frac{\cos(° i \bar{} _A)}{\sin(\bar{} _B i \bar{} _A)} & i\frac{\sin(° i \bar{} _A)}{\sin(\bar{} _B i \bar{} _A)} & 0 \\ 0 & 0 & 1 \end{bmatrix} \begin{Bmatrix} F_C^{\emptyset} \\ P^n \\ M \end{Bmatrix}$$

which is also compatible with Equation (3:6). Once it is substituted back to Equation (3:2), it can be shown that T is also linearly related to L by a set of linear equations. The linear mapping matrix will be referred as the J matrix:

$$\begin{Bmatrix} T_{A1} \\ T_{A2} \\ T_B \end{Bmatrix} = \begin{bmatrix} 0.5 & 0 & \frac{1}{2d\sin(\theta_A)} & \frac{-\cos(\phi-\theta_B)}{\sin(\theta_B-\theta_A)} & \frac{\sin(\phi-\theta_B)}{\sin(\theta_B-\theta_A)} & 0 \\ 0 & 0.5 & -\frac{1}{2d\sin(\theta_A)} & \frac{\cos(\phi-\theta_A)}{\sin(\theta_B-\theta_A)} & -\frac{\sin(\phi-\theta_A)}{\sin(\theta_B-\theta_A)} & 0 \\ 0 & 1 & 0 & 0 & 0 & 1 \end{bmatrix} \begin{Bmatrix} F_C \\ P^n \\ M \end{Bmatrix} \quad (3.9)$$

$$\{T\} = [J]\{L\}$$

E) General tensionability condition with arbitrary load

All of the con…gurations that have been investigated so far are restricted to a triple intersecting point between the cable axes and the spine axis. There are cases when these axes may not be able to intersect all the time. For a general case, let point O be the pivot point of the spine, ±x be the horizontal eccentric distance measured from the axis of the parallel cable joint to point O (positive if the intersection is between the spine axis and cable B), and ±y to be the vertical eccentric distance measured from the axis of cable B and point O (positive if the intersection is below point O). The cable robot shown in Figure 3-8 is the most general con…guration for this type of robot, and it is tensionable for any external force and torque by a …nite value of spine force if the following conditions are met:

$$C1: \theta_A - \theta_B < 180^\circ \quad (3.10)$$

$$C2: -180^\circ < \theta_B < \phi + 90^\circ < \theta_A < 0^\circ \quad (3.11)$$

$$C3: \left| \pm x + \pm y \frac{\cos(\phi-\theta_A)}{\cos(\phi-\theta_B)} \frac{\cos(\theta_B)}{\cos(\theta_A)} \right| < d \quad (3.12)$$

These conditions are designed to ensure a monotonic relationship between the cable tensions and the spine force. The equilibrium equations of the end-e¤ector show that the cable tensions are linearly related to the applied loads. Of all three components in the load vector, the e¤ective

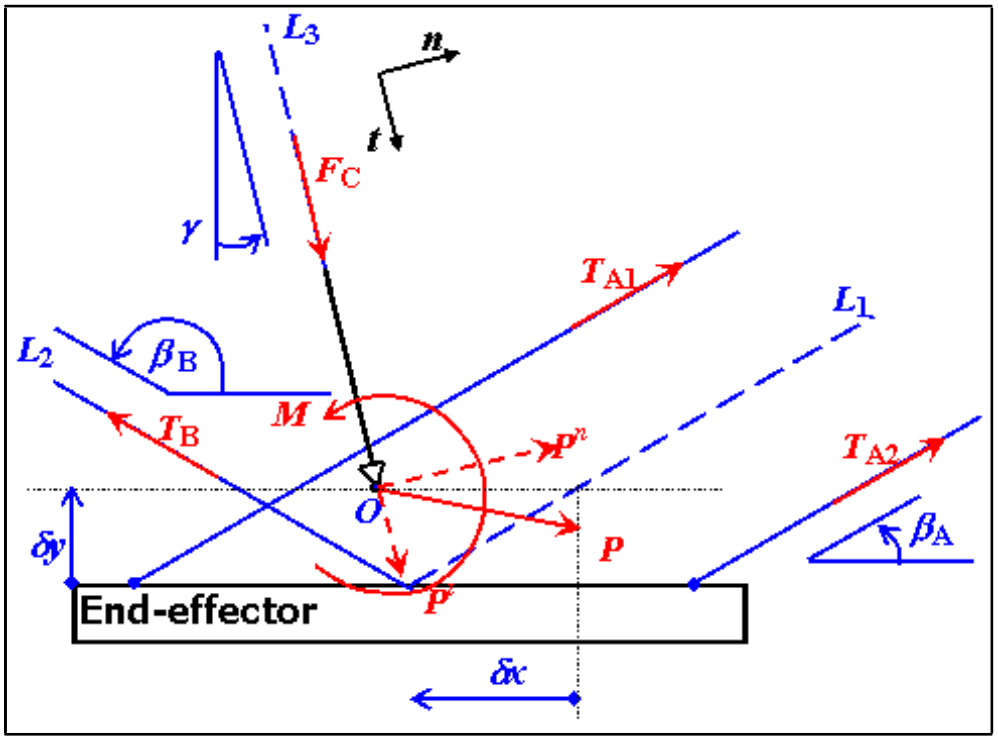

Figure 3-8: General cable-robot con…guration with eccentric distance

spine force, $F_C^{\emptyset}$ is the only directly controllable load. Since the objective is to obtain a positive cable tension with a positive spine force, one must ensure all cable tensions monotonically increase with the spine force. Mathematically speaking, the derivatives of the cable tensions with respect to the spine force must be positive.

The introduction of the eccentric distance generates a bias torque about point O. The e¤ect is two additional terms introduced in Equations (3:4). Therefore, the load to tension mapping function can be re-derived with the necessary update from Equations (3:6) and (3:9) accordingly. Incorporating the eccentricity terms in Equation (3:4)produces:

$$M = (T_{A1} - T_{A2})d\sin(\gamma_A) + (T_{A1} + T_{A2})(\pm y\cos(\gamma_A) - \pm x\sin(\gamma_A) + T_B \pm y\cos(\gamma_B) \quad (3.13)$$

With the new moment equilibrium equation, Equation (3:6)becomes:

$$\begin{Bmatrix} T_{A1} \\ T_{A2} \\ T_B \end{Bmatrix} = \begin{bmatrix} \frac{1}{2} - \frac{\pm x}{d} & \frac{1}{2}\frac{\pm y}{d}\frac{\cos(\theta_B)}{\sin(\theta_A)} & \frac{1}{2d\sin(\theta_A)} \\ \frac{1}{2} + \frac{\pm x}{d} & -\frac{1}{2}\frac{\pm y}{d}\frac{\cos(\theta_B)}{\sin(\theta_A)} & -\frac{1}{2d\sin(\theta_A)} \\ 0 & 1 & 0 \end{bmatrix} \begin{Bmatrix} T_A \\ T_B \\ M \end{Bmatrix} \tag{3.14}$$

Finally Equation (3:9) can be modified with the Equation (3:14):

$$\begin{Bmatrix} T_{A1} \\ T_{A2} \\ T_B \end{Bmatrix} = \begin{bmatrix} \frac{1}{2} - \frac{\pm x}{d} & \frac{1}{2}\frac{\pm y}{d}\frac{\cos(\theta_B)}{\sin(\theta_A)} & \frac{1}{2d\sin(\theta_A)} \\ \frac{1}{2} + \frac{\pm x}{d} & -\frac{1}{2}\frac{\pm y}{d}\frac{\cos(\theta_B)}{\sin(\theta_A)} & -\frac{1}{2d\sin(\theta_A)} \\ 0 & 1 & 0 \end{bmatrix} \begin{bmatrix} -\frac{\cos(\phi-\theta_B)}{\sin(\theta_B-\theta_A)} & \frac{\sin(\phi-\theta_B)}{\sin(\theta_B-\theta_A)} & 0 \\ \frac{\cos(\phi-\theta_A)}{\sin(\theta_B-\theta_A)} & -\frac{\sin(\phi-\theta_A)}{\sin(\theta_B-\theta_A)} & 0 \\ 0 & 1 & 0 \end{bmatrix} \begin{Bmatrix} F_C^{\perp} \\ P^n \\ M \end{Bmatrix} \tag{3.15}$$

The product of the middle matrix in Equation (3:15) forms the new J matrix. After some simplification, each column of the J matrix is shown below:

$$J_{i1} = \frac{1}{2d}\frac{\cos(\phi-\theta_B)}{\sin(\theta_B-\theta_A)} \begin{bmatrix} -\left[d - \pm x - \pm y\frac{\cos(\theta_B)}{\sin(\theta_A)}\frac{\cos(\phi-\theta_A)}{\cos(\phi-\theta_B)}\right] \\ \left[d + \pm x + \pm y\frac{\cos(\theta_B)}{\sin(\theta_A)}\frac{\cos(\phi-\theta_A)}{\cos(\phi-\theta_B)}\right] \\ 2d\frac{\cos(\phi-\theta_A)}{\cos(\phi-\theta_B)} \end{bmatrix}$$

$$J_{i2} = \frac{1}{2d}\frac{\sin(\phi-\theta_B)}{\sin(\theta_B-\theta_A)} \begin{bmatrix} \left[d - \pm x - \pm y\frac{\cos(\theta_B)}{\sin(\theta_A)}\frac{\sin(\phi-\theta_A)}{\sin(\phi-\theta_B)}\right] \\ -\left[d + \pm x + \pm y\frac{\cos(\theta_B)}{\sin(\theta_A)}\frac{\sin(\phi-\theta_A)}{\sin(\phi-\theta_B)}\right] \\ -2d\frac{\sin(\phi-\theta_A)}{\sin(\phi-\theta_B)} \end{bmatrix}$$

$$J_{i3} = \frac{1}{2d}\frac{1}{\sin(\theta_A)} \begin{bmatrix} 1 \\ -1 \\ 0 \end{bmatrix} \tag{3.16}$$

Due to the linear relationship between the cable tensions and the spine force, the derivatives of the cable tension with respect to the spine force is the first column of the J matrix in Equation (3:16). Therefore the tensionability condition can be ensured if J_{i1} are all positive, and the Inequality Equations (3:10) to (3:11) are designed to produces a positive J_{i1}. Conditions C1 and C2 in Equations (3:10) and (3:11) are geometric constraints that must be met in setting up the end-effector configuration. Satisfying these conditions automatically guarantees $\frac{\partial T_B}{\partial F_C^{\perp}}$

to be positive. The eccentric distance terms in Equation (3:16) can be interpreted as biases that shift the tension distribution amongst the parallel cable joint. Inequality Equation (3:12) in Condition C3 is designed to establish a minimum bound on the horizontal cable separation distance, d so that it can tolerate this shift in tension.

3.3 Application of the tensionability conditions and the equations of motion

The tensionability criteria investigated above emphasize one common feature; there exists a minimum, …nite spine force, F_C that generates rigid manipulator con…guration for a given bound on the external load. The design strategy of the manipulator is to …nd that minimum spine force and apply it to the entire workspace of the manipulator. The exact analysis would include the kinematics model of the entire robot. The cable tension can be determined by Equation 3.15. A design optimization procedure will most likely include …nding some mechanical parameters such as the maximum and minimum cable tensions, actuator torque powers given some constraints on the design speed and acceleration. This can be accomplished by evaluating the equations of motion and the equation of tensions using the minimum spine force at discrete points on the workspace. Once all of the relevance mechanical properties have been identi…ed, one can compute the performance index of the con…guration and apply standard optimization procedure to …nd the optimal robot con…guration. A detail design procedure is discussed in Chapter 4.

3.3.1 Insight into tensionability equations

There are only three (end-e¤ector) kinematical independent parameters in these equations, $F_C^{\emptyset}$, P^n, and M; these parameters form the load vector. The cable tension equations can be considered as a 3 by 3 transformation matrix that maps the dynamic force to the cable tension. There are two important insights to the cable tension equations. Firstly, the eccentric distances, $\pm x$ and $\pm y$ provide bias in the cable tensions of the parallel cable joint. This is bounded to increase the range of the cable tension under di¤erent dynamic and operating conditions. Therefore, eccentric distances should be avoided at all times. Secondly, the horizontal cable separation distance, d reduces the e¤ect of any applied torque and all other eccentric loads.

This e¤ectively reduces the asymmetric e¤ect on the system. One major drawback of a large d is the size of the end-e¤ector, which usually causes a larger inertia load. Therefore, the optimal design must be a balance between the cable separation distance and other constraints. Thirdly, the e¤ect of the applied torque is magni…ed with a small cable axes angle, $\bar{}_A$. The geometric interpretation of a small $\bar{}_A$ is the parallel cable joint starts to line up. This is e¤ectively a region that is close to the singular con…guration of the system. The minimum cable tension is expected to occur when the end-e¤ector is close to this critical point.

3.3.2 Rewriting the load vector in terms of the end e¤ector kinetics

The tensionability of the system must be met at any given velocity and acceleration of the end-e¤ector. Moreover, there should be a minimum cable tension speci…cation for safety purpose. Under the conditions listed in Section 3.2.1, there exists a minimum spine force to put the manipulator in a rigid pose. It is necessary to …nd this spine force before evaluating other mechanical performance indicators.

The dynamic equations stated in Equation (3:15)would be a good start. However, the load vector does not constitute a good choice of independent variable as there is no a priori knowledge regarding the P^n and the M acting on the end-e¤ector. Better choices of independent variables are the kinematics parameters such as maximum velocity and acceleration, as they are the natural measures of the robot performance. Therefore, it would be more convenient to express the cable tension vector from these kinematics parameters. In anticipation that a pneumatic cylinder is to be employed for the spine, this work derives the load vector from the inertia force that is produced by cylinders. This analysis is equally valid for any other revolute-prismatic-revolute (RPR) types of spine that produces a constant spine force. The friction and dampening e¤ect of the pneumatic cylinder are ignored for simplicity. The lower robot would now be composed of three rigid bodies: the cylinder body, the cylinder piston, and the end-e¤ector (the cables are considered as massless).

When a pneumatic cylinder is used as a spine, it can be considered as RPR linkage. The equations of motion can be derived from the Newton equation. Figure 3-9 shows the free body diagram of the two rigid bodies. In the FBD, F_C^0 denotes the force from the pneumatic air, F_C is the force that the piston deliver to the end e¤ector, and it is the equivalent to the spine

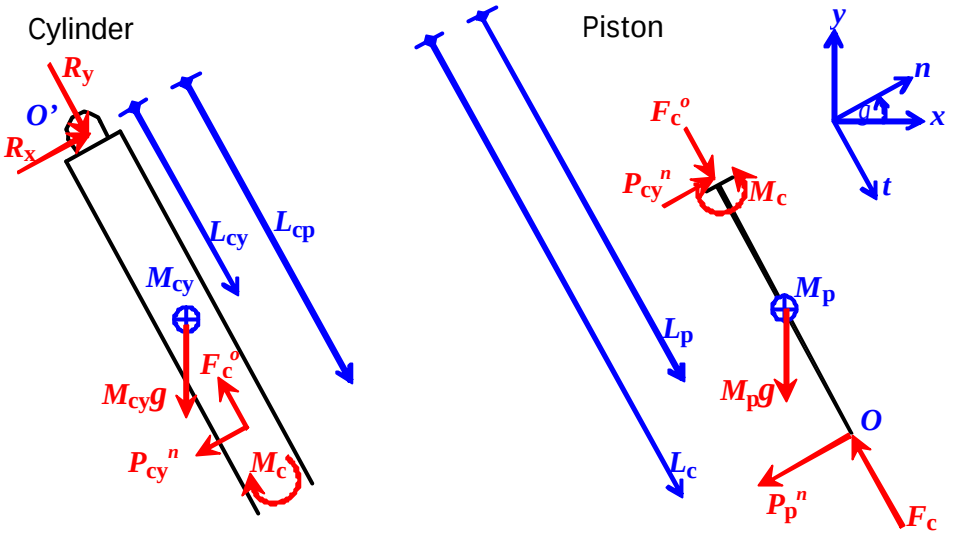

Figure 3-9: Free body diagram of the pneumatic cylinder as the spine element. All linear dimensions are measured from the pivot point O'

force discuses in Section 3.2.1. P_{cy} is the normal force that cylinder exerts on the piston interface, and P_p^n is the normal force that the piston exerts on the end-e¤ector. Note that P_p^n does not represent the P^n in the load vector, it is merely a contribution of P^n.

Starting from D'Alembert's principal, the acceleration of the cylinder can be calculated from the applied force and the inertia property. Then, isolate the forces, F_C and P_p^t that the piston exerts onto the end-e¤ector. The details mathematical manipulation are shown below. The mass component, M_{cy}, M_p, are the mass of the cylinder and piston respectively; similarly the inertia component I_{cy}^o, I_p^o, are the second moment of inertia with respect to the pivot point O^0. The dynamic force associated with the pneumatic cylinder is listed below:

For the tangential force, apply the force equilibrium on the piston:

$$F_C^o - F_C + M_p g\cos(\theta_c) - M_p(\ddot{L}_c - L_{cp}\dot{\theta}^2) = 0 \tag{3.17}$$

$$F_C = F_C^o + M_p\left[L_{cp}\dot{\theta}^2 - \ddot{L}_c + g\cos(\theta_c)\right] \tag{3.18}$$

For the normal force, apply the moment equilibrium on cylinder and the piston about the

pivot point O^0:

$$-M_c - P_{cy}^n L_{cp} - M_{cy} g \sin(\theta) L_{cy} - I_{cy}^o \ddot{\theta} = 0 \tag{3.19}$$

$$M_c + P_{cy}^n L_{cp} - M_p g \sin(\theta) L_p - P_p^n L_c - I_p^o \ddot{\theta} - 2M_p L_p \dot{L}_p \dot{\theta} = 0 \tag{3.20}$$

Adding Equation (3:19) and Equation (3:20) together produces:

$$-(M_{cy} L_{cy} + M_p L_p) g \sin(\theta) - P_p^n L_c - (I_{cy} + I_{po}) \ddot{\theta} - 2M_p L_p \dot{L}_p \dot{\theta} = 0 \tag{3.21}$$

The normal force can be isolated from Equation (3:21)

$$P_p^n = -\frac{1}{L_c}\left[I_{cy}^o + I_p^o \right] \ddot{\theta} + 2M_p L_p \dot{L}_p \dot{\theta} + (M_{cy} L_{cy} + M_p L_p) g \sin(\theta) \tag{3.22}$$

The other contribution of the load vector come from the end-effector. Consider Δx and Δy to be the eccentric distances between the center of gravity of the end-effector that mass M_e and the pivot point O (see Figure 3-10), one can compute the gravitational (static) and the inertia (dynamic) force that is associated with the end-effector. The magnitude and direction of the end effector acceleration is denoted by a and α_a; the magnitude and the direction of the end effector velocity is denoted by v and α_v. This inertia force can be translated to point O and resolved into the tangential component P^t, and normal component P_e^n. The rotary effect can be compensated with an equivalent torque which turns out to be the applied moment, M in the load vector.

$$P^t = M_e[a \sin(\alpha_a - \theta) + g \cos(\theta)] \tag{3.23}$$

$$P_e^n = -M_e[a \cos(\alpha_a - \theta) + g \sin(\theta)] \tag{3.24}$$

$$M = -M_e[a[\cos(\alpha_a)\Delta y + \sin(\alpha_a)\Delta x] + g\Delta x] \tag{3.25}$$

By the principal of superposition, the total applied load vector (F_C^0, P^n, M) is the summation of the force contributions from the cylinder in Equations 3.18 and 3.22 and the dynamic

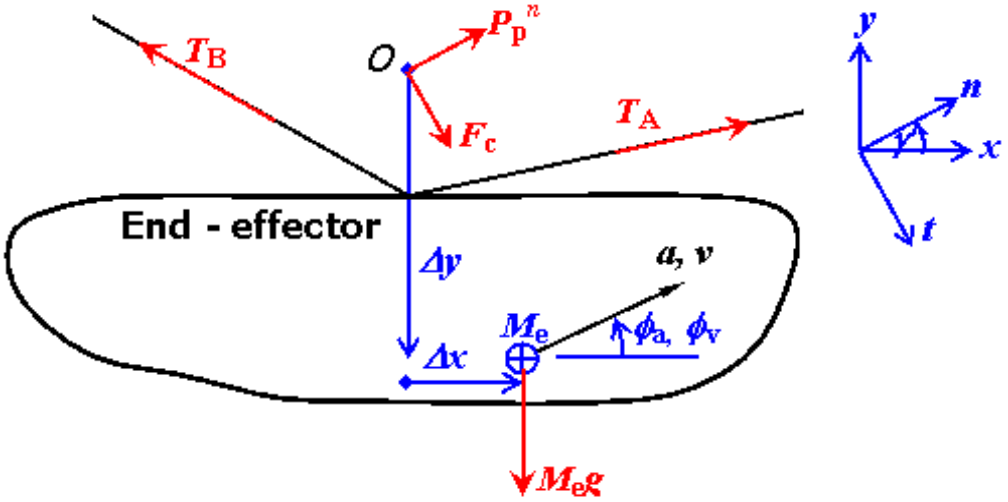

Figure 3-10: Free body diagram of the end-effector

force from the end-effector Equations in Equations 3.23 to 3.25. The following equations summarizes the computation of the load vector.

$$F_C^0 = M_e a \sin(\alpha_a - \theta) + M_p \left[L_{cp}\dot{\theta}^2 - \ddot{L}_c \right] + [M_e + M_p] g \cos(\theta_c) + F_C^o \tag{3.26}$$

$$P^n = -M_e a \cos(\alpha_a - \theta) - \left(\frac{I_{cy}^o + I_p^o}{L_c} \ddot{\theta} + 2M \frac{L_p}{L_c} \dot{L}_p \dot{\theta} \right) - (M_e + M_{cy} \frac{L_{cy}}{L_c} + M_p \frac{L_p}{L_c}) g \sin(\theta) \tag{3.27}$$

$$M = -M_e a [\cos(\alpha_a) \cdot y + \sin(\alpha_a) \cdot x] + M_e g \cdot x \tag{3.28}$$

3.3.3 Identifying the minimum spine force and the maximum cable tension

The objective of this analysis is to identify the minimum cylinder force that should be applied to the cylinder and the maximum cable tension that can occur at the cables; it is necessary to identify the worst case parameters that minimizes the cable tension. Since the cylinder is kinetically dependent on the end-effector, the kinetics of the cylinder should be expressed as the velocity and acceleration of the end-effector. Unfortunately, the complexity of the kinematics equations makes this problem becomes a computationally intensive optimization

problem; hence, it is not feasible to compute the exact tension minimizer. However, one can calculate the upper and lower limit of the each term as a function of the maximum allowable end-effector velocity, V_{max} and acceleration, A_{max}. The idea is to identify the range of the cylinder acceleration terms ($\ddot{A}$, $\ddot{L}_c$, $\dot{\theta}^2$, and $L_c\dot{\theta}$) in Equation (3:18) and Equation (3:22). The enveloping load values can be computed using the extremes value of each acceleration component.

Lets the origin of the cylinder be point O' and track the other end of the cylinder at point O. The velocity and the acceleration of the end-effector is denoted according to Figure 3-10. Expressions for L_c and θ can be derived by trigonometry:

$$L_c = \sqrt{x^2 + y^2} \tag{3.29}$$

$$\theta = \arctan\left(\frac{y}{x}\right) \tag{3.30}$$

For the time derivatives of L_c, use implicit derivative on $L^2 = x^2 + y^2$, and substitute in $L_c \sin(\theta)$, $-L_c \cos(\theta)$, $v\cos(\phi_v)$, and $v\sin(\phi_v)$ to x, y, $\dot{x}$, and $\dot{y}$ respectively. A simple expression of $\dot{L}_c$ is shown below:

$$\begin{aligned} \dot{L}_c &= \frac{x}{L_c}\dot{x} + \frac{y}{L_c}\dot{y} \\ &= \frac{v}{L_c}[x\cos(\phi_v) + y\sin(\phi_v)] \\ &= v[\sin(\theta)\cos(\phi_v) - \sin(\theta)\cos(\phi_v)] \\ &= -v[\sin(\phi_v - \theta)] \end{aligned} \tag{3.31}$$

For $\ddot{L}_c$, take derivative on first step of Equation (3:31), and use the same substitution on x, y, but substitute $a\cos(\phi_a)$ and $a\sin(\phi_a)$ to $\ddot{x}$ and $\ddot{y}$. A simple expression of $\ddot{L}_c$ is shown below:

$$
\begin{aligned}
\ddot{L}_c &= \frac{x^2}{L_c} + \frac{x}{L_c}\ddot{x} + \frac{y^2}{L_c} + \frac{y}{L_c}\ddot{y} - \frac{L_c^2}{L_c} \\
&= \frac{a}{L_c}[x\cos(\theta_a) + y\sin(\theta_a)] + \frac{v^2}{L_c} - \frac{v^2\sin^2(\theta_v - \theta)}{L_c} \\
&= a[\sin(\theta)\cos(\theta_a) - \cos(\theta)\sin(\theta_a)] + \frac{v^2}{L_c}\left[1 - \sin^2(\theta_v - \theta)\right] \\
&= -a\sin(\theta_a - \theta) + \frac{v^2}{L_c}\cos^2(\theta_v - \theta)
\end{aligned} \tag{3.32}
$$

Similarly, for $\dot{\theta}$, take the derivative using the chain rule, and use the same substitution as above. A simple expression of $\dot{\theta}$ is shown below:

$$
\begin{aligned}
\dot{\theta} &= \frac{1}{1 + \left(\frac{y}{x}\right)^2}\left[-\frac{y}{x^2}\dot{x} + \frac{\dot{y}}{x}\right] \\
&= \frac{1}{L_c^2}[y\dot{x} - x\dot{y}] \\
&= -\frac{v}{L_c}[\cos(\theta)\cos(\theta_v) + \sin(\theta)\sin(\theta_v)] \\
&= -\frac{v}{L_c}[\cos(\theta_v - \theta)]
\end{aligned} \tag{3.33}
$$

For $\ddot{\theta}$, apply derivative on Equation (3:33) before the substitution Then, use the same substitution described above. A simple expression of $\ddot{L}_c$ is shown below:

$$
\begin{aligned}
\ddot{\theta} &= -\frac{2L_c}{L_c^3}[y\dot{x} - x\dot{y}] + \frac{1}{L_c^2}[y\ddot{x} - x\ddot{y}] \\
&= \frac{2L_c}{L_c^2}v[\cos(\theta)\cos(\theta_v) + \sin(\theta)\sin(\theta_v)] - \frac{a}{L_c^2}[\cos(\theta)\cos(\theta_a) + \sin(\theta)\sin(\theta_a)] \\
&= \frac{2L_c}{L_c^2}v[\cos(\theta - \theta_v)] - \frac{a}{L_c^2}[\cos(\theta - \theta_a)] \\
&= -\frac{2v^2}{L_c^2}\sin(\theta_v - \theta)\cos(\theta - \theta_v) - \frac{a}{L_c^2}[\cos(\theta - \theta_a)]
\end{aligned} \tag{3.34}
$$

It is convenience to have an $\dot{\theta}^2$ and $L_c\dot{\theta}$ expression because these terms appear frequently

in Equations (3:18)and (3:22) as the centrifugal and Coriolis acceleration. From Equations (3:31)and (3:33), these expressions are:

$$\dot{\theta}^2 = \frac{v^2}{L_c^2}\cos^2(\alpha_v - \theta) \tag{3.35}$$

$$L_c\ddot{\theta} = \frac{v^2}{L_c}\frac{\sin(2(\alpha_v - \theta))}{2} \tag{3.36}$$

Since $\sin(\mu) \in [-1, 1]$ and $\cos^2(\mu) \in [0, 1]$, the extreme accelerations can be computed from Equations (3:32)to (3:36). The ranges of these acceleration terms are:

$$0 \le \dot{\theta}^2 \le \frac{V_{max}^2}{L_c^2} \tag{3.37}$$

$$-\frac{V_{max}^2}{L_c} \le 2L_c\ddot{\theta} \le \frac{V_{max}^2}{L_c} \tag{3.38}$$

$$-A_{max} \le \ddot{L}_c \le A_{max} + \frac{V_{max}^2}{L_c} \tag{3.39}$$

$$-\left(\frac{V_{max}^2}{L_c^2} + \frac{A_{max}}{L_c}\right) \le \ddot{\alpha} \le \frac{V_{max}^2}{L_c^2} + \frac{A_{max}}{L_c} \tag{3.40}$$

The enveloping load value can be computed by applying the upper (lower) bound of the acceleration on Equation (3:26), (3:27), and (3:28). Table 3.1 summarizes the combination of these acceleration terms in computing the extremum of the load vector.

The linearity properties of the dynamic equations guarantees the minimum spine force exists at the extremum of the load parameters. By rearranging Equation (3:15) and (3:26), one can compute a set of linear equations to find the minimum cylinder force, F_C^{min}. The following procedure [1] can be used to identify the F_C^{min} of a particular robot pose given a certain value of minimum cable tension, T^{min}.

Step 1: Calculate $F_C^{\alpha} = (M_p + M_e)(g\cos(\theta) - A_{max}) - M_p\frac{V_{max}^2}{L_c}$

[1] This procedure assumes the tensionablilty condition described in previous section has been met.

Table 3.1: Parameter to calculate the enveloping Load Vector

Load	Eq'n	Value	Centrifual ω^2	Coriolis $2\dot{L}_c\omega$	Tangential $\dot{\omega}L_c$	Angular $\dot{\omega}$	End E¤ector (dynamic)
F_c^0	3.26	Min	Lower	N/A	Upper	N/A	$-M_e A_{max}$
		Max	Upper	N/A	Lower	N/A	$M_e A_{max}$
P^n	3.27	Min	N/A	Upper	N/A	Upper	$M_e A_{max}$
		Max	N/A	Lower	N/A	Lower	$-M_e A_{max}$
M_o	3.28	Min	N/A	N/A	N/A	N/A	$-M_e A_{max} \begin{bmatrix} -\phi x \\ -\phi y \end{bmatrix}$
		Max	N/A	N/A	N/A	N/A	$-M_e A_{max} \begin{bmatrix} -\phi x \\ \phi y \end{bmatrix}$

Step 2: for k=1..3, set $P_k^n = \begin{cases} \text{Maximize } P^n \text{ if } J_{k2} \cdot 0 \\ \text{Minimize } P^n \text{ otherwise} \end{cases}$;

$M_{ok} = \begin{cases} \text{Maximize } M \text{ if } J_{k3} \cdot 0 \\ \text{Minimize } M \text{ otherwise} \end{cases}$;

Step 3: Calculate $F_C^{min} \cdot \max_k \left(\frac{T_k^{min} - J_{k;2} P^n - J_{k;3} M_k}{J_{k;1}} - F_C^{\alpha} \right)$

Proof. The in…mum cylinder (spine) force is the force that set the cable tension to a minimum tension T^{min}. From Equation (3:15), $T_k = \{J_k^c \{L\}$, or $F_C^{\emptyset} = \frac{T_k^{min} - J_{k;2} P^n - J_{k;3} M_k}{J_{k;1}}$. The cylinder force, F_C^o can be isolated from Equation (3:26) and produces:

$$F_C^o = \frac{T_k^{min} - J_{k;2} P^n - J_{k;3} M_{ok}}{J_{k;1}} - F_C^{\alpha} \tag{3.41}$$

where F_C^{α} is computed as in step 1, and Equation (3:41) is similar to the expression in step 3. A tensionable cable system implies $J_{k;1} > 0$. Therefore, the in…mum cylinder force occurs when the normal and torque terms takes the most negative value as illustrated in step 2. However, Equation (3:41) computes the minimum cylinder force for just one cable. It is necessary to …nd the biggest F_C^o amongst the three cables to ensure all three cable wire meets the minimum cable tension requirement. Therefore, the minimum necessary cylinder force is the maximum of all F_C^o. ■

Another important quantity is the maximum cable tension T^{max} when the in…mum cylinder

force is applied to the end-e¤ector. Unlike the computation of the in…mum cylinder force, the maximum cable tension analysis requires the load vector to maximize its value. Therefore, its process is almost opposite of computing T^{min}. Equation (3:15) suggests the following procedure to calculate T^{max}:

Step 1: Calculate F_c^0 = Maximize(F_c^0)

Step 2: for k=1..3, set

$$P_k^n = \begin{cases} \text{Minimize } P^n \text{ if } J_{k2} \cdot 0 \\ \text{Maximize } P^n \text{ otherwise} \end{cases};$$

$$M_{ok} = \begin{cases} \text{Minimize } M \text{ if } J_{k3} \cdot 0 \\ \text{Maximize } M \text{ otherwise} \end{cases};$$

Step 3: Calculate $T_k^{max} \cdot \begin{bmatrix} 0 \\ \vdots \\ 0 \end{bmatrix} \begin{bmatrix} F_C^0 \\ P_k^n \\ M_k \end{bmatrix}$;

Chapter 4

Design Considerations and Optimization Method

The proposed planar pick-and-place manipulator has 2 translational DOFs, X (forward/backward), and Y (up/down). Since a general purpose programmable manipulator generally does not have any preference in operating orientation, it is reasonable to expect the optimal design has some sort of symmetry about the Y axis. From the functional points of view, the robot must be both sti¤ and light enough to satisfy the cycle rate and repeatability requirement, moreover, the robot should not take up too much space, yet its workspace should be relatively large for a di¤erent operating environment. All of these factors posed di¤erent completing design factors which a designer must compromise. This chapter explores some typical design considerations and a design strategies for the proposed planar manipulator.

4.1 Design Constraints and Criteria

Two design constraints are the usable workspace and the tensionability within the workspace. The former constraint is purely a geometric issue, and it involves the overall robot topology. The later constraint is local to the end-e¤ector and is addressed in Chapter 3. Typical workspace is speci…ed as the width and height of a rectangle. The actual dimension of the workspace is heavily dependent on the application. In this work, the dimension of the workspace is set to be a 700mm by 100mm rectangle.

As for performances, the manipulator should be driven at high speed with a minimal amount of power. As far as speed is concerned, the ability to accelerate would be a better indicator since the acceleration and deceleration phase is likely to dominate the trajectory for high speed machine. Another advantage of using acceleration as an speed indicator is that acceleration provides other mechanical conditions that may be useful for evaluating the cost function. Moreover, spatial consideration such as machine footprint should also be integrated in the decision process. This is because space is usually a precious resource in an typical industrial environment. The relevance spatial measurements include the robot width and the robot height. The performance indicators of interest are summarized as follow:

- The footprint (width) of the con…guration, w
- The height of the con…guration, h
- The minimum cylinder force, F_c^{min}
- The maximum cable tension, T^{max}
- The maximum actuator power, W^{max}
- The maximum actuator e¤ort, M^{max}
- The maximum positional error factor, $\pm P^{max}$

4.2 Optimization Methods Overview

The particular implementation calls for a pneumatic cylinder as the spine element. It is assumed that the cylinder force is held constant across the entire workspace. The proposed optimization algorithm consists of two layers, the inner layer concerns with feasibility issue while the outer layer optimizes the geometric and design parameters of the manipulator. Since feasibility is a system constraint, the inner optimization process must be able to identify the global extremum for the respective parameters. While modern optimization algorithms are relatively e¢cient on global convergence, they do not guarantee to convergence to the global extremum [3]. Unless the particular robot kinematics produces a spatial monotonic relationship with the feasibility related properties, a sequential search would be a more appropriate method for the inner optimization

process. As for the outer optimization process, geometric parameters are the parameters of interest. Since they are the criteria for comparison purpose only, an e¤ective optimization process should be used to …nd the optimal or a near optimal solution. In order to increase the possibility of obtaining the global optimal con…guration, the outer optimization process has to be repeated multiple times at di¤erent starting point for a complete optimization search.

A set of mechanical indicators are evaluated for each con…guration, the overall cost function can be a weighted sum of these cost indicators. Some of them, namely the mechanical indicators described in Section 4.3 can be measured by the extreme value and the mean of the extreme value. The extreme values are of particular importance as they dictate the speci…cation of the mechanical component. The mean extreme values should also be considered as they are better representation for the overall mechanical resource to be allocated for a robot con…guration to operate at its maximum performance. In this work, the purposed optimization scheme are performed in two phases. The …rst phase computes the local optimal con…gurations from a given set of start points based on the extreme indicators values only. In the second phase, a …ner grid is used in the inner optimization process, and the mean extreme values as well as the absolute indicator extreme values are used for computing the manipulator cost. The starting point of the second phase optimization are the local optimal con…guration obtained in the previous phase.

4.3 Computation of the necessary mechanical indicators- the inner optimization process

The purpose of the inner optimization process is to provide the feasibility information and the mechanical performance index. Feasibility can be ensured if the manipulator forms a rigid pose across its entire workspace. Under certain conditions enlisted in Section 3, the manipulator is always in a rigid mode regardless of the external load. Hence they will achieve tensionability as long as there is a su¢cient amount of cylinder force to balance the external load. This work assumes a particular con…guration fails to met the tensionability criterion if any entry in …rst column of the J matrix is negative as explained in Section 3.2.1. When such a violation

to occurs, the inner process should either terminate the optimization process (hard constrain), or output some exponentially large value as it approaches the infeasible con…guration (barrier function). The implementation of the actual inner optimization process is depended on the design of the outer optimization process.

As mentioned above, it is critical to …nd the global optimizer on several mechanical properties (F_c^{min}, T^{max}, W^{max}) in the inner optimization layer, it is more appropriate to solve this layer by a sequential search. The idea is to discretize the workspace into a lattice of vertices, and evaluate the mechanical properties at each and every vertex until the extreme value is found. To implement the algorithm in a computationally e¤ective manner, it is advantageous to have an initial pass to computing the J matrix by Equation (3:15) at each vertex. Tensionability and other mechanical properties can be computed easily from the J matrix afterward.

4.3.1 Inverse kinematics and the basic Mechanical properties

Before executing the inner optimization process, one should derive the inverse kinematics model and the cable axis expressions which are needed when computing the J matrix. Both of these expressions map the workspace coordinate to its respective space coordinate:

$$\mu = \mu(x;y); \quad \mu \mu f : R^2 ¡ > R^2 \tag{4.1}$$

$$^{-} = ^{-}(x;y); \quad ^{-} \mu f : R^2 ¡ > R^2 \tag{4.2}$$

The inverse kinematics equation, μ in Equation (4:1), and the cable axes equation $^{-}$ in Equation (4:2) are depended on the upper robot assembly and its design parameters. Moreover, the computation of the equation of motions also require the cylinder length L_c in Equation (3:29) and the spine axis angle ° Equation (3 ¡ 9), which is somewhat independent from the upper robot assembly as long as a RPR type of spine is used. In the initial pass of the inner process, one should calculate the J matrix at each vertex of the grid. If the con…guration were not inherently tensionable (as described in case E of Section 3.2.1), the inner optimization process should store the minimum value of J_i. This is needed later in global convergence. At the same time, the minimum cylinder force, F_c^{min} can be computed by the procedure shown in 3.3.3.

Once the J matrix have been obtained and the F_c^{min} has been determined, other basic mechanical properties can be computed hereafter. It is essential to compute the global F_c^{min} before computing other mechanical indicator such as the maximum cable tension (using the biggest minimum necessary cylinder force of all poses) as most of these indicators monotonically increases with the cylinder force. A typical scenario is to …nd the worst case mechanical indicators at a bounded end-e¤ector acceleration. In this case, the dynamic e¤ect of the cylinder (central assembly) could be signi…cant. A possible procedure to compute the minimum required cylinder force and the maximum cable tension at a given pose is shown in Section 3.3.3.

4.3.2 Computation of the Positional Error Factor

Another important performance index is the positional error factor, ±P. The positional error factor is de…ned to be the maximum amount of the positional error ($\tilde{x}$, $\tilde{y}$) in the workspace coordinate when there is a slight deviation of actuator angle ($\tilde{\mu}_1;\tilde{\mu}_2$) on the robot actuator space. In this work, a …rst order approximation technique is used to approximate the error. The mathematical formulation is shown as follow:

$$
\begin{aligned}
\pm P &= \frac{1}{\tilde{\mu}_1\ \tilde{\mu}_2} \left(\sup_{\|(\tilde{\mu}_1\ \tilde{\mu}_2)\| < \varepsilon} \begin{Bmatrix} \tilde{x} \\ \tilde{y} \end{Bmatrix} \right) \\
&= \frac{1}{\tilde{\mu}_1\ \tilde{\mu}_2} \left(\sup_{\|(\tilde{\mu}_1\ \tilde{\mu}_2)\| < \varepsilon} \left\{ \begin{Bmatrix} x(\mu_1+\tilde{\mu}_1;\mu_2+\tilde{\mu}_2) \\ y(\mu_1+\tilde{\mu}_1;\mu_2+\tilde{\mu}_2) \end{Bmatrix} - \begin{Bmatrix} x(\mu_1;\mu_2) \\ y(\mu_1;\mu_2) \end{Bmatrix} \right\} \right)
\end{aligned}
\tag{4.3}
$$

Apply the …rst order approximation on the perturbation term in Equation (4:3), ±P simpli…es to:

$$
\begin{Bmatrix} \tilde{x} \\ \tilde{y} \end{Bmatrix} = \begin{Bmatrix} x(\mu_1;\mu_2) \\ y(\mu_1;\mu_2) \end{Bmatrix} + \left(\begin{Bmatrix} (\mu_1;\mu_2) \\ (\mu_1;\mu_2) \end{Bmatrix} \begin{Bmatrix} \tilde{\mu}_1 \\ \tilde{\mu}_2 \end{Bmatrix} \right) + O(2)
$$

$$
\frac{1}{4} \begin{bmatrix} \frac{dx}{d\mu_1} & \frac{dx}{d\mu_2} \\ \frac{dy}{d\mu_1} & \frac{dy}{d\mu_2} \end{bmatrix} \begin{Bmatrix} \tilde{\mu}_1 \\ \tilde{\mu}_2 \end{Bmatrix}
$$

$$\pm P = \frac{\sup \left\| J_v \begin{Bmatrix} \tilde{\mu}_1 \\ \tilde{\mu}_2 \end{Bmatrix} \right\|}{\left\| \begin{matrix} \mathbf{j} & \mathbf{k} \\ \tilde{\mu}_1 & \tilde{\mu}_2 \end{matrix} \right\|} \tag{4.4}$$

where J_v is the Manipulator (Velocity) Jacobian.

One small problem is that the forward kinematics equation for parallel mechanism is usually a set of implicit equations or a set of relatively complex expressions. This raises runtime issue when they are computed directly, and let alone the computation of their Jacobian matrix. Fortunately, it is possible to compute the Jacobian matrix from the inverse kinematics as well, this is known as the inverse velocity analysis [9]. Moreover, it turns out that part of this computation is also required in computing the maximum actuator torque and power in Section 4.3.3. Therefore, this indirect approach does not add too much computation burden in the overall analysis.

Suppose Equation (4:1) have been derived, the …rst order approximation on some small perturbation in the workspace coordinate suggests an set of equivalent equations that is similar to the J_v:

$$\begin{Bmatrix} \mu_1(x+\tilde{x}; y+\tilde{y}) \\ \mu_2(x+\tilde{x}; y+\tilde{y}) \end{Bmatrix} = \begin{Bmatrix} \mu_1(x;y) \\ \mu_2(x;y) \end{Bmatrix} + \delta\mu \begin{Bmatrix} \tilde{x} \\ \tilde{y} \end{Bmatrix}$$
$$\begin{Bmatrix} \tilde{\mu}_1 \\ \tilde{\mu}_2 \end{Bmatrix} = \begin{bmatrix} \frac{d\mu_1}{dx} & \frac{d\mu_1}{dy} \\ \frac{d\mu_2}{dx} & \frac{d\mu_2}{dy} \end{bmatrix} \begin{Bmatrix} \tilde{x} \\ \tilde{y} \end{Bmatrix} \tag{4.5}$$

It follows that the manipulator Jacobian matrix, J_v is the inverse of the inverse kinematics gradient function, $[\delta\mu]^{-1}$:

$$J_v = [\delta\mu]^{-1} \tag{4.6}$$

From Equation (4:4), it follows that the positional error factor is some form of the norm of $[\delta\mu]^{-1}$. This work assumes the positional deviation is caused by an independent normally

distributed random error in the actuators. As a result, the norm to be employed is the square of the (matrix) euclidean norm, which makes ±P become a proportional constant between the positional deviation and a normally distributed actuator errors. In some applications, a designer may require to design a manipulator against the worst case scenario. In those cases, a 1-norm would be a more appropriate choice as it makes ±P become a measurement of positional deviation due to a uniformly distributed random actuator errors.

$$\pm P = \left\| [5\mu]^{i-1} \right\|_2^2 \tag{4.7}$$

Since the positional error factor is to be evaluated at every node of the inner optimization process, it may be a good idea to simplify the computation as much as possible. Mathematically speaking, the euclidean norm is the same as the largest singular value of the $[5\mu]^{i-1}$, which is also equal to the square root of the largest eigenvalue of $\left(5\mu^{i-1}\right)^T \left(5\mu^{i-1}\right)$. Since $\left(5\mu^{i-1}\right)^T \left(5\mu^{i-1}\right) = \left(5\mu^T\ 5\mu^{i-1}\right)$ is a positive de…nite matrix providing the manipulator is not in a singular pose, it can be shown that the matrix inversion step in Equation (4:7) is not necessary. An equivalent equation is:

$$\pm P = \frac{1}{\min\left|\mathrm{eig}\left|5\mu\ 5\mu^T\right|\right|} \tag{4.8}$$

4.3.3 Maximum Actuator E¤ort and Power

Another mechanical indicator to be explored is the maximum actuator e¤ort and power. The following analysis is based on a rotary actuator and the rotary e¤ort - Torque. The same analysis is equally valid with linear actuator and linear e¤ort - force. Unlike other mechanical parameters, the actuator e¤orts and powers involve a signi…cant amount of dynamic force from the upper robot assembly. Consider a cable is attached to an (rotary) actuator i through a rigid linkage, the torque that the actuator deliver to the system M_i the power that the actuator delivers to the system W_i can be calculated by the following equation:

$$M_i = T_i \pounds L_i + I_i \ddot{\mu}_i + m_i \bar{L}_i \cos(\mu) g \tag{4.9}$$

$$W_i = M_i \mu_i \tag{4.10}$$

where, μ_i is the direction of rotation measured from horizontal

T_i is the cable tension

L_i is the length of the moment arm of the rigid linkage

$\bar{L}_i$ is the distance between the center of mass of the rigid linkage and the pivot point

I_i is the mass moment of inertia of the rigid linkage

m_i is the mass of the rigid linkage

This torque is the summation of the applied torque from the cable, the inertia torque from the rigid linkage, and the gravitational force from the mass of the linkage. The actual maximum joint torque is difficult to compute in general, however it is possible to establish an upper bound on the joint power by assuming the maximum applied torque coexists with the maximum inertia torque. Since there is no limitation imposed on the joint speed and acceleration, it is necessary to relate the joint kinetics to the workspace kinetics. The expressions can be obtained from taking the time derivative on the inverse kinematics equations (4:1) as shown below:

$$\dot{\mu}_i = \nabla \mu_i(x;y) \begin{Bmatrix} \dot{x} \\ \dot{y} \end{Bmatrix} = \begin{bmatrix} \frac{\partial \mu_i}{\partial x} & \frac{\partial \mu_i}{\partial y} \end{bmatrix} \begin{Bmatrix} \dot{x} \\ \dot{y} \end{Bmatrix} \tag{4.11}$$

$$\ddot{\mu}_i = \nabla \mu_i(x;y) \begin{Bmatrix} \ddot{x} \\ \ddot{y} \end{Bmatrix} + \begin{bmatrix} \dot{x} & \dot{y} \end{bmatrix} H(\mu_i(x;y)) \begin{Bmatrix} \dot{x} \\ \dot{y} \end{Bmatrix} = \begin{bmatrix} \frac{\partial \mu_i}{\partial x} & \frac{\partial \mu_i}{\partial y} \end{bmatrix} \begin{Bmatrix} \ddot{x} \\ \ddot{y} \end{Bmatrix} + \begin{bmatrix} \dot{x} & \dot{y} \end{bmatrix} \begin{bmatrix} \frac{\partial^2 \mu_i}{\partial x^2} & \frac{\partial^2 \mu_i}{\partial x \partial y} \\ \frac{\partial^2 \mu_i}{\partial x \partial y} & \frac{\partial^2 \mu_i}{\partial y^2} \end{bmatrix} \begin{Bmatrix} \dot{x} \\ \dot{y} \end{Bmatrix} \tag{4.12}$$

Table 4.1: The extremum value from the second joint acceleration expression

Case	Positive De…niteness	Eigenvalue	Supremum	In…mum
1	Positive De…nite	$\lambda_1 > 0$ $\lambda_2 > 0$	$V_{max}^2 \lambda_1$	0
2	Positive Semide…nite	$\lambda_1 > 0$ $\lambda_2 = 0$	$V_{max}^2 \lambda_1$	0
3	Inde…nite	$\lambda_1 > 0$ $\lambda_2 < 0$	$V_{max}^2 \lambda_1$	$V_{max}^2 \lambda_2$
4	Negative Semide…nite	$\lambda_1 = 0$ $\lambda_2 < 0$	0	$V_{max}^2 \lambda_2$
5	Negative De…nite	$\lambda_1 < 0$ $\lambda_2 < 0$	0	$V_{max}^2 \lambda_2$

Since the magnitude of the end-e¤ector velocity and acceleration are bounded by V_{max} and A_{max}, the maximum actuator velocity and acceleration can be obtained by solving the constrained optimization equations. First consider the joint velocity, it is in a linear form with respect to the end-e¤ector acceleration. From linear algebra, the supremum and in…mum of the expression is $k5\mu_i k_2 V_{max}$.

As for the joint acceleration expression in Equation (4:12), it consists of two linearly independent expressions. The extremum of $\ddot{\mu}_i$ exists at the extreme value of these expressions. The …rst expression is related to the direct acceleration, and it is in a linear form with respect to the end-e¤ector acceleration. Therefore, the magnitude of the …rst term is bounded by $k5\mu_i k_2 A_{max}$. The second joint acceleration expression is related to Christo¤el symbols, and it is in a quadratic form with respect to the end-e¤ector velocity. Since the Hessian of smooth function is always symmetrical, the extreme values from the second expression are related to on the eigenvalues, λ of the Hessian matrix. There are several possibilities on the resulting extremum values in a quadratic form listed in the table below:

An observation from Table 4.1 shows that the extremum values of the second expression are $V_{max}^2 \max(\lambda; 0)$ and $V_{max}^2 \min(\lambda; 0)$. The following equations concisely compute the joint kinetics extremum:

$$\dot{\theta}_i^{+} = V_{max} k_5 \mu_i k_2 \tag{4.13}$$

$$\ddot{\theta}_i^{+} = A_{max} k_5 \mu_i k_2 + V_{max}^2 \max(\alpha_{max}; 0) \tag{4.14}$$

$$\dot{\theta}_i^{i} = -V_{max} k_5 \mu_i k_2 \tag{4.15}$$

$$\ddot{\theta}_i^{i} = -A_{max} k_5 \mu_i k_2 + V_{max}^2 \min(\alpha_{min}; 0) \tag{4.16}$$

Equations (4:13) and (4:14) are the supremum of the joint velocity and acceleration while Equation(4:15) and (4:16) are the in…mum counterpart.

Typical actuators do not have a preference on the operating direction, except for double acting cylinder which provides slightly more force in the pushing direction than in the pulling direction. Therefore, it is reasonable to assume that the torque capacity of the actuator is the bigger of the forward torque and the reverse torque. From the computational points of view, it is slightly more e¢cient to compute the reverse torque to be a positive value in the reverse direction. Since the tension component always provides a forward torque, a maximum reverse torque must occur with a minimal tension and the most negative acceleration. Above arguments result in the following equation that computes the maximum actuator torque capacity, and it always produce a positive number:

$$M_i^{max} = \max\left(T_i^{max} \pounds L + I_i \ddot{\theta}_i^{+} + m_i L_i \cos(\mu) g; -T_i^{min} \pounds L - I_i \ddot{\theta}_i^{i} - m_i L_i \cos(\mu) g\right) \tag{4.17}$$

If further assumption is made on the amount of the sinking power being the same as the amount of the sourcing power in an actuator, the maximum power capacity of the actuator i would be the higher of the sinking power and the sourcing power. In this case, the reverse torque should be considered as a negative torque in the forward direction as indicated in the

following equation:

$$W_i^{max} = \max\left(T_i^{max} \pounds L + I_i \ddot{\mu}_i^{+} + m_i L_i \cos(\mu) g \dot{\mu}_i^{+};\ T_i^{min} \pounds L + I_i \ddot{\mu}_i^{i} + m_i L_i \cos(\mu) g \dot{\mu}_i^{i} \right) \tag{4.18}$$

Note that Equation 4.18 produces a positive number when multiplied with a negative velocity for comparisons purpose.

4.4 Computation of the desired geometrical and performance factor - the outer optimization process

Since the outer optimization concerns with performance only, a simple and e¤ective direct search optimization algorithm such as the simplex method would be a better choice to identify a set of apparent optimal system parameters. This step requires the kinematics model of the entire robot, hence, the topology of the upper robot must be known. A simplex algorithm and other direct search methods are described in [22].

Direct search algorithms typically do not produce the global optimal solution. Thus, this outer optimization is run multiple times to increase the probability of obtaining the global optimal con…guration. The n-parameters that are required to constrain a robot con…guration is denoted to be $X \frac{1}{2} R^n$. In this work, a variation of the simplex algorithm is chosen for optimization purpose. To set up a simplex algorithm, an initial robot con…guration X_0 should be chosen in random in the …rst phase of optimization. Feasibility should be checked for the initial con…guration. If the con…guration is feasible, a set of n + 1 robot con…gurations that forms a convex-hull near to X_0 is chosen as the initial simplex. One way to choose such a set of con…gurations is to add a small normalized deviation to X_0 in random. The small deviation can be generated by a Gaussian distribution routine (and normalized afterward) for an unbiased result. The resulting simplex does not always inscribe X_0, but its centroid will be closed to the feasible con…guration. Regardless of how these robot con…gurations were generated, it is essential to check for feasibility on each and every single con…guration as there is no guarantee that the newly generated points are also feasible points. Once the initial simplex is chosen, the simplex algorithm can begin to execute. Upon the convergence of the simplex, the best

con…guration amongst the n + 1 points is saved for the second phase of analysis.

4.4.1 Modi…ed Dynamic Simplex Algorithm

Simplex algorithm, just like any other direct search method can guarantee a global convergence to a stationary point only if there is a su¢ciently rich set of feasible search direction [21, p1076]. This is particular challenging if there is a non-linear and/or if there is no a priori knowledge on the constraint function. Although modern direct search algorithm, utilizing stochastic technique provides a stronger convergence characteristic [4], they are relatively di¢cult to implement and often require several expert parameters for the …nest performance. Therefore, this work implements a simple dynamic simplex algorithm with L1 logarithmic penalty function to achieve a near optimal result.

Instead of establishing the entire constrained optimization method, it would be more straightforward to introduce the unconstrained simplex search algorithm. Let $F(X)$ be the design cost function to minimize and Y^i be the cost value of the i^{th} con…guration in the simplex set X^i, the Nelder and Meld simplex algorithm calls for successive re‡ection on the most costly con…guration [23]. For the purpose of completeness, the algorithm is reproduced with speci…c elaborations on this design problem.

The Nelder and Meld Simplex:

Set $K = 0$

Step 1: Re‡ection Step

Let X^{min} and X^{max} be the least and most costly con…guration and $\bar{X}^1$ be the centroid (mean) of all n + 1 con…gurations, compute $X_{ref} = 2\bar{X}^1 - X^{max}$.

Step 2: Contraction / Expansion step

case 1: If $F(X_{ref}) < F(X^{min})$, attempt expansion :

$$\begin{pmatrix} X_{new} \\ K \end{pmatrix} = \begin{cases} \begin{pmatrix} 2X_{ref} - \bar{X}^1 \\ 0 \end{pmatrix} & \text{if } F\left(2X_{ref} - \bar{X}^1\right) < F(X_{ref}) \\ \begin{pmatrix} X_{ref} \\ 0 \end{pmatrix} & \text{otherwise} \end{cases}$$

case 2: if $F(X_{ref}) > F(X^{max})$, attempt contraction

$$\begin{pmatrix} X_{new} \\ K \end{pmatrix} = \begin{cases} \begin{pmatrix} \frac{X_{ref} + X^{max}}{2} \\ 0 \end{pmatrix} & \text{if } F\left(\frac{X_{ref} + X^{max}}{2}\right) < F(X^{min}) \\ \begin{pmatrix} \frac{X_{ref} + X^{max}}{2} \\ K+1 \end{pmatrix} & \text{if } F(X^{min}) \cdot F\left(\frac{X_{ref} + X^{max}}{2}\right) < F(X^{max}) \\ \begin{pmatrix} X_{ref} \\ n+1 \end{pmatrix} & \text{otherwise} \end{cases}$$

Step 3: Replace the vertex

If $K < n+1$, replace X^{max} with X_{new}

otherwise contract the entire simplex: set $X_i = \frac{(X_i + X^{min})}{2}$

Step 4: Check for convergence

Here the characteristic norm of the simplex is de…ned to be the largest Euclidean distance between the simplex centroid and its vertices. If the characteristic norm is below a certain prede…ned threshold γ^{max}, the simplex algorithm is said to be converged and the result of the search is X^{min}. Otherwise, go back to Step 1

However, the design problem requires a constrained optimization algorithm. In order to avoid hitting the infeasible region, a modi…ed objective function that takes the degree of the admissibility into consideration is employed. This approach is known as the L1 penalty method [22]. The underlying principal is to add a penalty cost as the searching sequence approaches the boundary of an inequality constraint, but the penalty is de-weighted as the sequence converges [22]. Lets $F(X)$ and $C(X)$ be the cost function to be minimized and the constraint function for which a feasible con…guration would produce a positive value, the e¤ective objective function can be written as a weighted sum between $F(X)$ and $C(X)$:

$$G(x) = F(X) + \mu \log(C(X)) \tag{4.19}$$

The weighting parameter ^{1}, is designed such that it will asymptotically approach to zero as the search sequence converges. In this case, the weighting parameter can be the characteristic norm of the simplex described in Step 4 of the above simplex algorithm. This penalty approach prevents the search sequence from stepping over the constraint boundary, while introducing minimal amount of disturbance to the cost function during the search. The simplex algorithm enlisted above can be adopt by simply replacing the F (X) with G(X).

4.5 Summary of the Optimization process

There are three distinct steps in the designed optimization process. The …rst step is the outer optimization that uses a modi…ed Nelder and Meld simplex to optimize the geometric parameters. This outer optimization step is to be repeated for a predetermined number of times to obtain a set of promising starting points for further analysis in step 3. For a manipulator design that has n parameters, Flow Chart 1 shows the implementation of the outer optimization. The second step of the optimization process is used to calculate the cost of a design. In this step, a sequential search technique is employed to calculate the mechanical parameters within the workspace. An e¢cient (for computation time) method to calculate these mechanical parameters is documented in Flow Chart 2. The last step is the detail analysis step that is essentially a second pass of the …rst two steps with two enhancements:

i) The detail analysis begins with the best con…gurations from the previous analysis.

ii) The detail analysis uses a denser mesh and looks for the mean of the mechanical performance indicators in the inner optimization.

The overall optimal design is the con…guration that has the lowest cost value in the analysis.

Figure 4-1: Outter optimization of geometric parameters

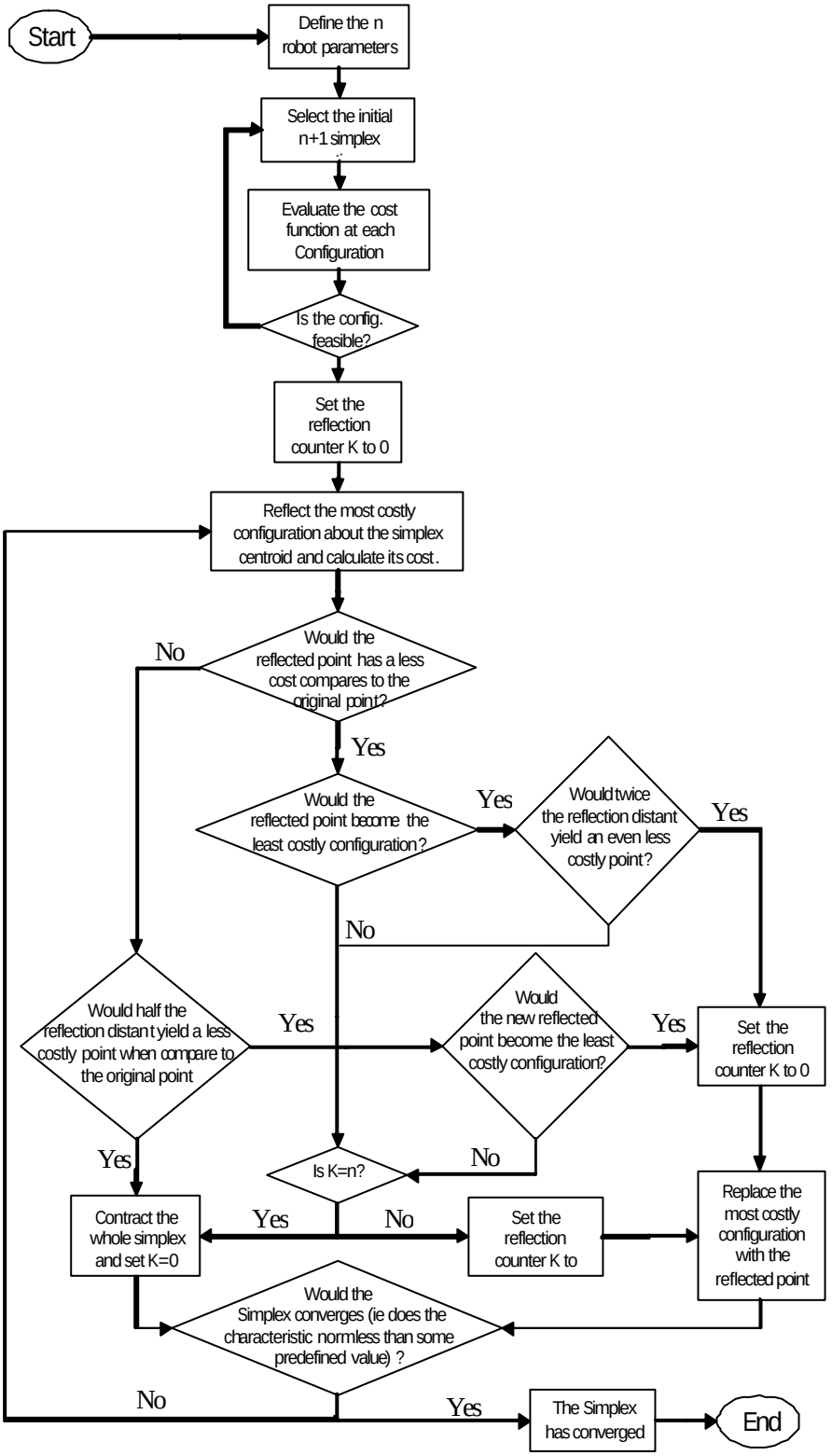

Figure 4-2: Inner optimization of the mechanical parameters

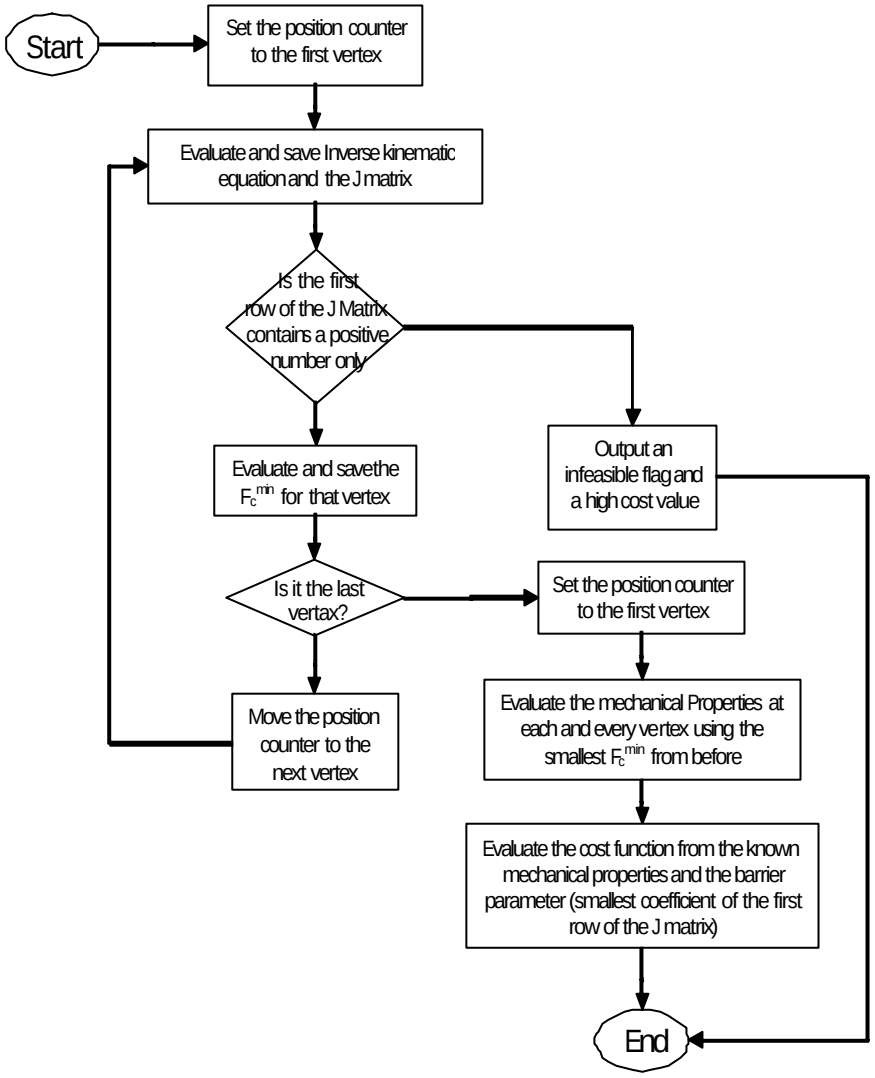

Chapter 5

Mechanical Design of Cable Based Planar Robot

Even with a nice conceptual design and a sound implementation strategy, this work would not be completed without showing some typical optimal design result. The purpose of the chapter is twofold, …rstly it gives comprehensive examples of the proposed parallel cable robot implementation; secondly, it is the backbone of building a cable robot prototype to evaluate the concept experimentally. Due to some historical background of this project, the actual prototype does not have the optimal con…guration as illustrating later in this chapter. One important tool that has been neglected in this work is a general strategy to come up with the inverse kinematics equations for this kind of parallel mechanism which has been somewhat addressed in the recent literature. A general workspace analysis of a board class of 2D parallel manipulator can be found in [24] and [6].

This chapter will explore two planar cable manipulator designs. Both of them utilize a pneumatic cylinder as the spine and two rotary actuators to manipulate the end-e¤ector. This analysis assumes that the spine force is held constant across the entire workspace. The inverse kinematics equations for these designs will be discussed for deriving the equations of the enveloping actuator torque and power. The workspace considered in this study is a 700mm by 100mm rectangle and the maximum velocity and acceleration of the end-e¤ector is set to 4:0m=s and 4g respectively. Also, the operating cable tension is set to be no less than 1N.

The performance indicators of interest are:

- footprint (width) of the con…guration
- height of the con…guration
- minimum cylinder force
- maximum cable tension
- maximum actuator power

There are some standard mechanical components which has a signi…cant amount of mass to dictates the dynamic behaviour of the robot. In both designs, it is assumed that a 25:4mm diameter, 2mm wall thickness aluminium cylinder tube is as used as the cylinder body. The length of the cylinder tube is set to be the same as the distance measured from the top of the workspace to the cylinder upper pivot. The center of mass is assumed to be at its geometric center. The cylinder piston is to be constructed by two 6:35mm diameter steel rods, and they should be long enough to cover the necessary stroke. The end-e¤ector is assumed to be a 40mm wide by 5mm thick aluminium plate, and its length is set to be equal to twice the horizontal cable separation distance, d. The horizontal and vertical distance measured from the pivot point O to the combine center of mass of the end-e¤ector and the 500g payload should be within §1cm and §5cm respectively.

5.1 Design 1: 2D-Deltabot

The …rst design uses a pair of rotational linkages to actuate the end-e¤ector. In this design, the cables do not change in length, and we will refer to them as a passive cables [16],[17]. Figure 5-1 is a pictorial view of the proposed design. This con…guration is kinematically similar to the Deltabot, and this works will refer to it as the 2D-Deltabot [17].

Section 3.3 discusses the negative impacts of the end-e¤ector eccentric distances. In this design, these eccentric distances are eliminated by attaching the cables to the end-e¤ector through revolute joints. The design parameters of this mechanism include the motor separation

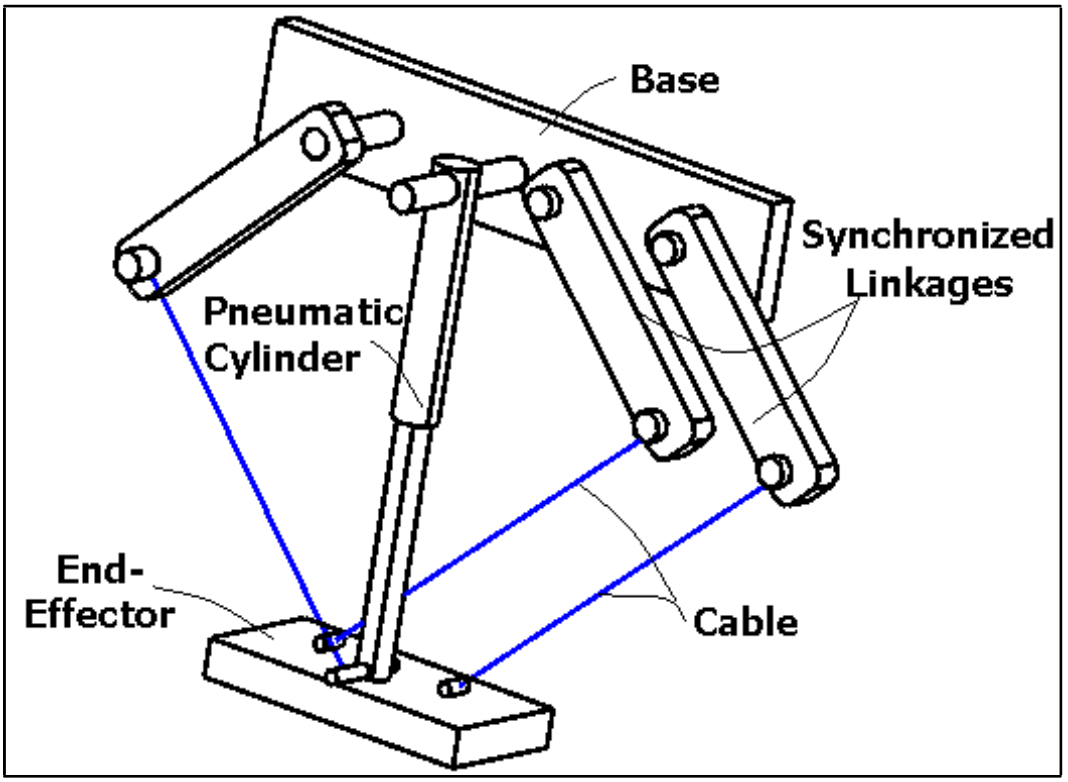

Figure 5-1: Pictorial View of 2D-Deltabot

distance (L_0), the length of the …rst linkage (L_1), the length of the cable (L_2), the minimum operation height (Y^{min}), the top cylinder operating o¤set (dH_c), and the cable separation distance (d). In anticipation that the optimal design is symmetrical about its center axis, the linkage on both actuators are assumed be the same size. From the kinematics point of view, the synchronized linkage can be replaced with an equivalent linkage midway between the paired linkages. The reachable workspace of the con…guration is shown in Figure 5-2. Note that the 2D-Deltabot has a convex workspace boundary at the bottom and a concave boundary at the top [12]. A concave work space boundary is disadvantageous as it is ine¢cient to allocate a rectangular workspace inside the convex space.

The kinematics model for 2D-Deltabot is similar to the Rice Planar Delta Robot [10] [6]. Derived from geometry, the following equation is the inverse kinematic equations for side A (the parrallel cable joint side).

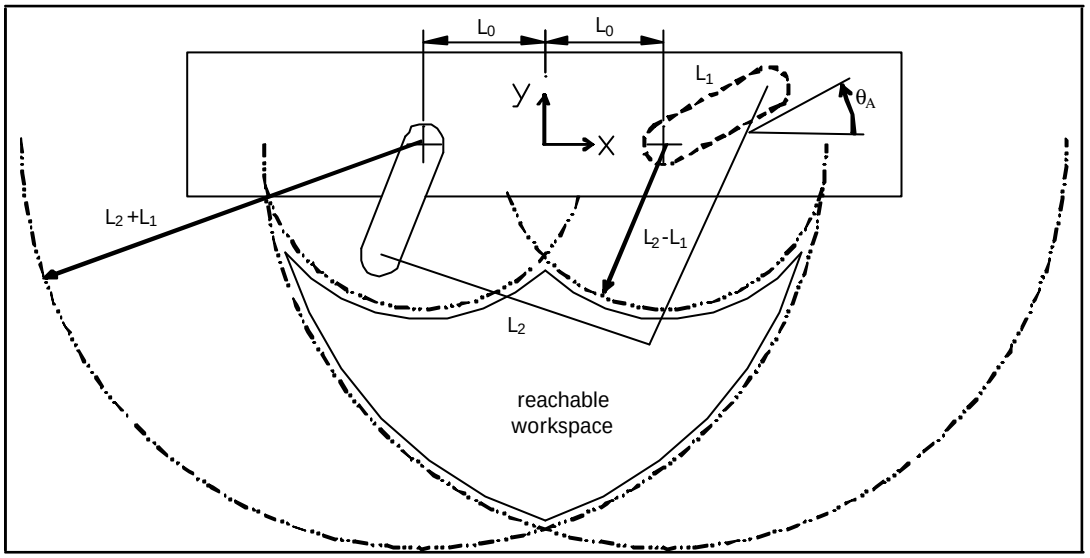

Figure 5-2: Workspace analysis of the 2D-Deltabot

$$\mu_A(X;Y) = \arccos\left(\frac{L_1^2 + Y^2 + (L_0 - X)^2}{2L_1\sqrt{Y^2 + (L_0 - X)^2}}\right) + \arctan\left(\frac{Y}{L_0 - X}\right) - \frac{\pi}{2} \qquad (5.1)$$

Due to the symmetry about the Y-axis, the second inverse kinematics equation, $\mu_B(X;Y)$ is $\mu_A(-X;Y)$.

Section 4.3 discussed a method to calculate the enveloping mechanical power from the actuator using the Gradient and the Hessian of the inverse kinematics equation. Let $A = \sqrt{X^2 + Y^2}$, and $Q_a = \sqrt{\frac{L_1^2 - L_2^2 + A^2}{4L_1A^2 - (L_1^2 - L_2^2 + A^2)^2}}$, the corresponding equations for side A of 2D-Deltabot are shown below:

$$\nabla\mu_A = -\frac{1}{A^2}\left(Q_a \begin{Bmatrix} L_o - X \\ -Y \end{Bmatrix} + \begin{Bmatrix} L_o - X \\ Y \end{Bmatrix}^{\perp}\right) \qquad (5.2)$$

$$H_{11} = 2\frac{L_0 - X}{A^2}\left(\frac{\partial \mu_A}{\partial X} - \frac{Q_a(L_0 - X)}{L_1^2 - L_2^2 - A^2}\left(1 + Q_a^2\frac{L_1^2 + L_2^2 - A^2}{L_1^2 - L_2^2 - A^2}\right)\right) + \frac{Q_a}{A^2} \quad (5.3)$$

$$H_{12} = -2\frac{Y}{A^2}\left(\frac{\partial \mu_A}{\partial X} - \frac{Q_a(L_0 - X)}{L_1^2 - L_2^2 - A^2}\left(1 + Q_a^2\frac{L_1^2 + L_2^2 - A^2}{L_1^2 - L_2^2 - A^2}\right) - \frac{1}{2Y}\right)$$

$$H_{22} = -2\frac{Y}{A^2}\left(\frac{\partial \mu_A}{\partial Y} - \frac{Q_a Y}{L_1^2 - L_2^2 - A^2}\left(1 + Q_a^2\frac{L_1^2 + L_2^2 - A^2}{L_1^2 - L_2^2 - A^2}\right)\right) + \frac{Q_a}{A^2}$$

Due to symmetry, the corresponding Gradient and Hessian equations for side B computed using the expressions from side A are:

$$5\mu_B(X;Y) = \begin{bmatrix} -\frac{\partial \mu_A}{\partial X}(-X;Y) & -\frac{\partial \mu_A}{\partial X}(-X;Y) \end{bmatrix} \quad (5.4)$$

$$H_B(X;Y) = \begin{bmatrix} \frac{\partial^2 \mu_A}{\partial X^2}(-X;Y) & -\frac{\partial^2 \mu_A}{\partial X \partial Y}(-X;Y) \\ -\frac{\partial^2 \mu_A}{\partial X \partial Y}(-X;Y) & \frac{\partial^2 \mu_A}{\partial Y^2}(-X;Y) \end{bmatrix} \quad (5.5)$$

5.1.1 Design rating and optimization result for 2D-Deltabot

The weighting for the design merit in the initial study is tabulated in Table 5.1. Typical mid-size servo DC brushless motor delivers 3Nm to 8Nm or torque. This is not enough to drive this con…guration. Therefore, a gear-reducer is a necessary component in this design. As a result, the maximum actuator torque is not critical. The best 60 (distinct) con…gurations from the initial optimization process were reprocessed with a …ner inner mesh resolution. Table 5.2 shows the top 6 distinct con…gurations based on the established cost function. Since most of these optimal results are very close from one to another, it is reasonable to assume that the global optimal result has been reached. The optimal con…guration requires 127N of central cylinder force. Using a 25:4mm pneumatic cylinder as the spine element, the robot can operate on roughly 2:5barof compressed air. Furthermore, the maximum cable enveloping tension is 127N. A Ø2mm steel cable wire can easily withstand this level of force [1]. As for spatial performance, the footprint of the robot is 913mm for a 700mm wide workspace. This is more than 75% spatial e¢ciency.

Although the design procedure is targeted to minimzise the absoulte and the average cable

Table 5.1: Weighting on various perfomance index of Deltabot

	Geometric		Mechanical Properties			
	w	h	F_c^{min}	T^{max}	W^{max}	E^{max}
unit	/mm	/mm	/N	/N	/W	r=mm
Abs	0.5	0.1	5	1	1	50
Mean	N/A	N/A	N/A	10	10	20

Table 5.2: The top 10 con…gurations and the associating performance index for 2D Deltabot

	Con…guration						Performance					
	L_0	L_1	L_2	dHc	Y^{min}	d	w	h	F_c^{min}	T^{max}	W^{max}	E^{max}
	mm	mm	mm	mm	mm	mm	mm	mm	N	N	W	mm=r
1	202	239	688	29	-574	101	983	574	127	127	648	93
2	195	238	683	28	-571	98	964	571	119	128	648	95
3	177	235	666	23	-599	89	913	559	124	130	651	99
4	190	235	672	25	-560	95	945	560	121	289	653	94
5	162	233	659	19	-557	81	871	557	128	132	652	105
6	196	236	674	27	-559	98	962	559	119	128	657	92

tension and actuator power, a study in the critical tension distribution over the workspace provides some insight to the design. Figure 5-3 shows the contour plot of the maximum tensionon on the cable of side B. Due to symmetry about the Y-axis, the cable tension on side B is the same as the equivalent cable tension on the parallel cable joint when the end-e¤ector is on the oppositie side of the workspace. Since there is only one cable on side B (the single cable size), the maximum cable tension will always be carried by Cable B. A simulation of the optimal cable tension shows that the worst case cable tension occurs near to the top center and the opposite lower corner of the workspace. The actuator power is profoundly dependent on cable tension; as a result, the maximum actuator power occurs near the maximum cable tension. Figure 5-4 shows a contour plot for maximum actuator power on actuator B.

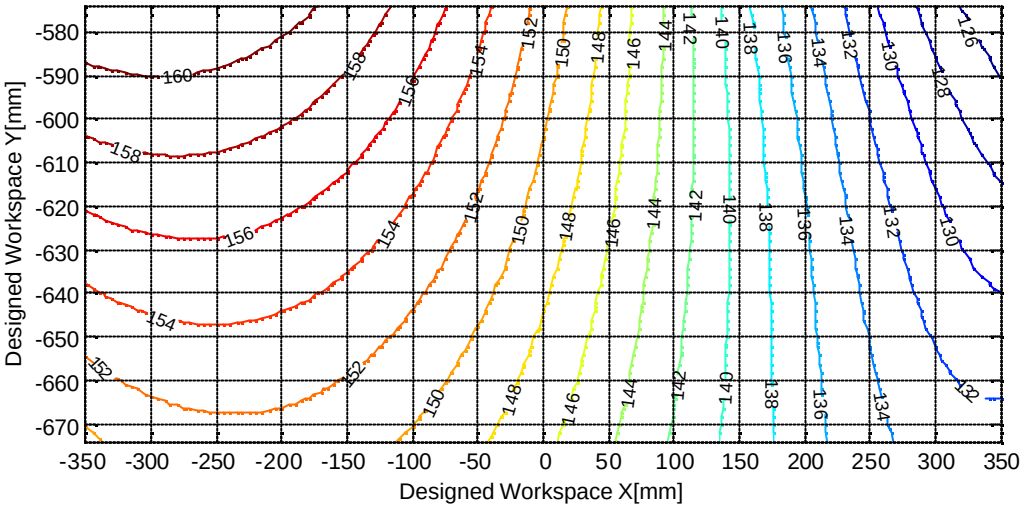

Figure 5-3: Maximum enveloping cable tension (occurs on the Side B) [N] for the optimal 2D-Deltabot con…guration.

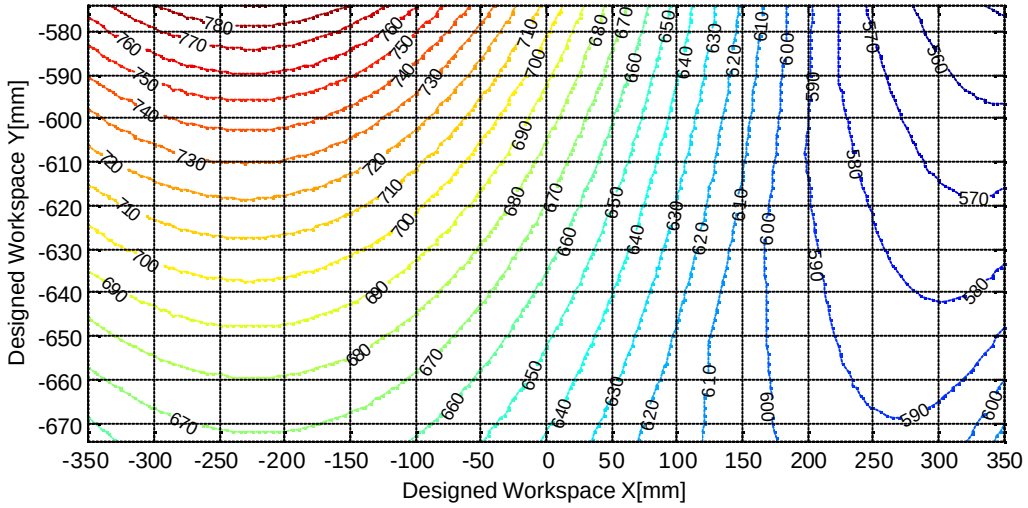

Figure 5-4: Maximum enveloping actuator power [W] of side B for the optimal 2D-Deltabot con…guration.

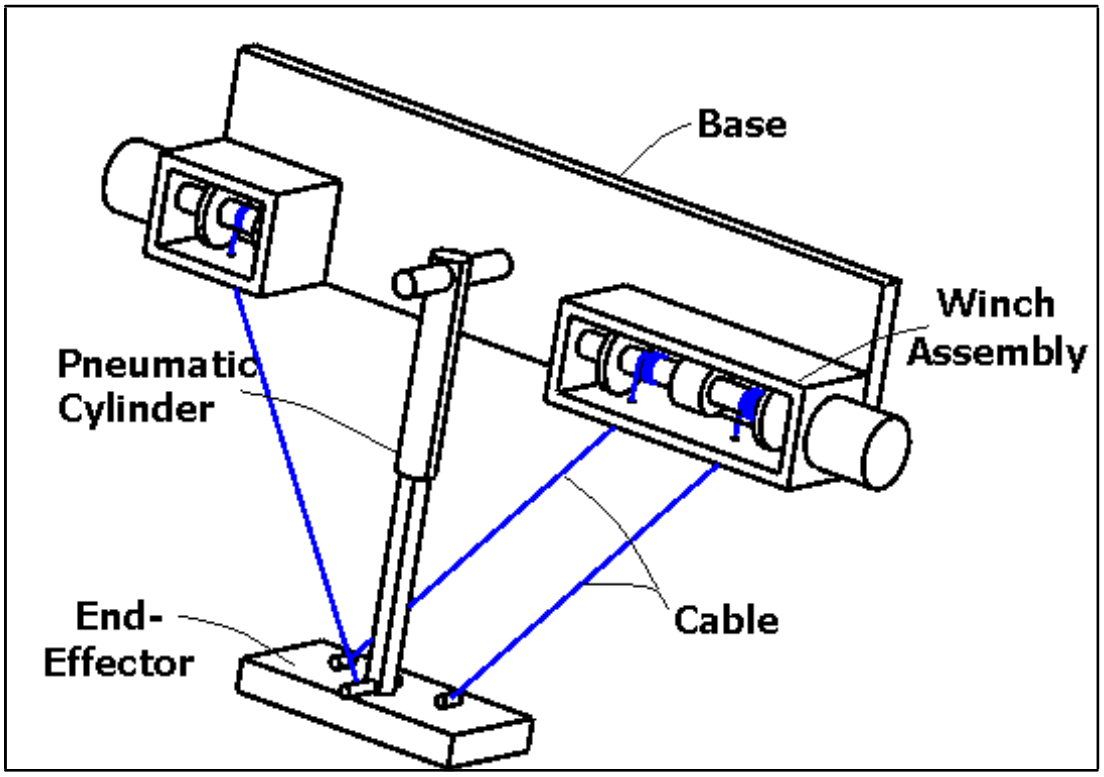

Figure 5-5: Pictorial View of 2D-Betabot. Note the bending radius is not shown for simplicity.

5.2 Design 2: 2D-Betabot

The second design utilises a winch to actuate the end-e¤ector. In this design, the cable lengths are controlled by the winch, and we will refer to them as active cables [16],[17]. Figure 5-5 is a pictorial view of the proposed design. and this works will refer this design as the 2D-Betabot [17].

Moreover, there will be a round bending surface at the cable attachment points. If there are two di¤erent cable bending radii on the upper and lower attachment point, there are 6 design parameters in this design: the motor separation distance (L_0), the upper bending radius (R_u), the lower bending radius (R_l), the minimum operation height (Y^{min}), the top cylinder operating o¤set (dH_c), and the cable separation distance (d). The bending surface can be constructed from a cable pulley. This feature eliminates the need for revolute joints which increases the reliability of the mechanism. The radius of curvature for the bend should be at least 45 times bigger than

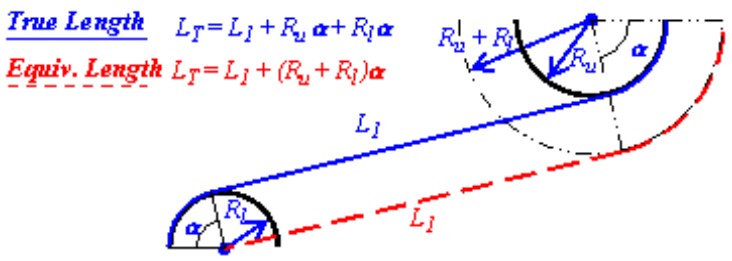

Figure 5-6: Equivalent Cable length can be obtained by translating the bending radius.

the radius of the steel cable to avoid bending fatigue [1]. However, this bending radius introduces eccentric distances at the end-e¤ector. From Section 3.3, this feature is going to compromise the cable joint torque capacity. As a result, there is a competing factor between a thicker cable and a smaller bending radius. The problem is that the cable thickness is determined by maximum cable tension, which in turn is a¤ected by the kinematics of the robot. Instead of solving this implicit constraint analytically, one alternative approach is to force a logarithmic barrier of the minimum bending radius constraint on the cost function. This approach is similar to the penalty method implemented in the optimization process, which prevent the search sequence from stepping over a constraint boundary without adding a signi…cant impact on the cost function.

Since the kinematics of this robot is new to the best of the author's knowledge, a detail derivation of the kinematics equations is needed in this work. Analogous to the workspace analysis of the 2D- Deltabot, the parallel cable joint is replaced by an equivalent linkage in this analysis. The two bending radii can be simpli…ed by perpendicularly translating the cable by R_l. This equivalent cable wraps around an equivalent pulley with radius R_T and hence maintains the same overall length as the original cable. Due to the geometric constraints, this equivalent cable always passes through the center of the lower bending radius, see Figure 5-6 for illustration.

Figure 5-7 shows the reachable workspace of the robot. Unlike 2D-Deltabot, 2D-Betabot has a concave workspace. There are three limiting boundaries on the reachable workspace. The top boundary is established by a horizontal line that is just below the lowest point of a circle with a radius equal to the total cable bending radius R_T; similarly the left and right boundaries

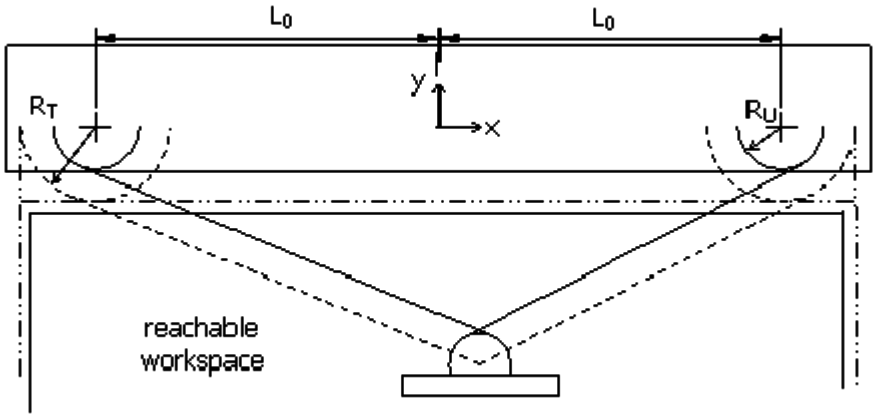

Figure 5-7: Workspace analysis of the 2D-Betabot

are established by the two vertical lines passing the extreme side of that circle. The robot will violate condition C1 if the end-e¤ector is on or above the top boundary and the end-e¤ector will disengage from the pulleys if it is not between the left and right boundaries. The lower bound of the workspace is limited by the amount of cable in the winch or the stroke length of the pneumatic cylinder only.

The total cable length is determined from two sections, the straight cable L_{x1} and the wrap-around cable L_{x2}. On side A, consider the triangle formed by the joint center, the cable take o¤ point, and the center of the end-e¤ector, the straight section of the cable can then be derived from pythrogen theorem as:

$$L_{A1} = \sqrt{(L_0 - X)^2 + Y^2 - R_T^2} \tag{5.6}$$

The calculation of the wrap-around section requires computing the angle that the amount of cable that are in contact with the pulley. Using the same triangle, the wrap-around cable length on side A is:

$$L_{A2} = R_T \left(\pi - \arctan\left(\frac{Y}{L_0 - X}\right) - \arctan\left(\frac{L_{A1}}{R_T}\right) \right) \tag{5.7}$$

Due to the symmetry about the Yaxis, the equivalent cable length of side B, L_B is $L_A(-X; Y)$: The Gradient and the Hessian maxtrix of the cable length can be computed from the sum of Equations (??) and (5:7). Let A be the distance between the center of the upper and the lower pulley, the Gradient and the Hessian of the Betabot can be computed by the following equations:

$$A = \sqrt{(L_0 - X)^2 + Y^2}$$

$$\nabla L_A = \frac{1}{A} \left(\frac{\partial L_{A1}}{\partial \begin{Bmatrix} X \\ Y \end{Bmatrix}} + R_T \begin{Bmatrix} \frac{X - L_0}{L_0 - X} \\ \frac{Y}{L_0 - X} \end{Bmatrix} \right)^T \tag{5.8}$$

$$H_A = \begin{bmatrix} \frac{L_0 - X}{A^2} \left(\frac{\partial L_A}{\partial X} + \frac{L_0 - X}{L_{A1}} + \frac{L_{A1}}{L_0 - X} \right) & -\frac{Y}{A^2} \left(\frac{\partial L_A}{\partial X} + \frac{L_0 - X}{L_{A1}} - \frac{R_T}{Y} \right) \\ -\frac{Y}{A^2} \left(\frac{\partial L_A}{\partial X} + \frac{L_0 - X}{L_{A1}} - \frac{R_T}{Y} \right) & \frac{Y}{A^2} \left(-\frac{\partial L_A}{\partial Y} + \frac{Y}{L_{A1}} + \frac{L_{A1}}{L_0 - X} \right) \end{bmatrix} \tag{5.9}$$

In this design, pivot point O is misaligned with the cable axes as in shown in Figure 3-8. Lets assumes the pivot point coincides with the center of the lower pulley of side B, the cable horizontal cable eccentric distance, $\pm x$ can be computed by extending the equivalent cable A to the horizontal line that passes through the pulley center axis. Using the sign convention from Section 3.2.1, this eccentric distance is always positive. Similarily, the vertical cable eccentric distance, $\pm y$ is the intersection of cable B and the vertical line that passes though the pulley center axis. This distance is also positive in sign. The numerical calcuation of these eccentric distances are as follows:

$$\pm x = \frac{R_l}{\sin(\theta_A)} \tag{5.10}$$

$$\pm y = -\frac{R_l}{\cos(\theta_B)} \tag{5.11}$$

Since the effect of eccentric distances is residual terms on the J matrix, substituting Equations (5:10) and (5:11) to Equation (3:15) shows that the magnitude of the cable axis angles,

¯ has a signi…cant e¤ect on the torque capacity. Therefore, it is expected that the operating workspace should be further below the upper pulley's level to maximize the torque capacity. Moreover, is it possible to reduce this side e¤ect by placing the pivot point closer to the the cable take o¤ points of the lower pulleys. However, this approach will introduce two additional design parameters in the optimization process and increase the search magnitude by two full order. As an initial study, it have been decided that no eccentric compensation should be made on the end-e¤ector.

5.2.1 Design rating and optimization result for 2D-Betabot

Table 5.3 shows the design weighting for this con…guration and Table 5.4 shows the top 6 (distinct) con…gurations based on the established cost function. The optimal con…guration requires 157N of central cylinder force. Assuming a one inch pneumatic cylinder is to be used, the mechanism operates on approximately 45psi of compressed air. While the 2D-Betabot design has compatible mechanical indicators such as maximum cable tension and actuator power when compared to the 2D-Deltabot counterpart, the 2D-Betabot con…guration performs poorly from the spatial performance point of view. The optimization results show that the 2D-Betabot design requires up to 50% more footprint and a 300% wider end-e¤ector when compared to the optimal 2D-Deltabot. Furthermore, the pulley radius is concentrated near the lower end of the allowable limits. It is evidable that the wide foot print is partial due to a signi…canly larger end-e¤ector, which in turn is caused by lower torque capacity.

Table 5.3: Weighting on various perfomance index of Betabot

	Geometric		Mechanical Properties			
	w	h	F_c^{min}	T^{max}	W^{max}	E^{max}
unit	/mm	/mm	/N	/N	/W	mm=mm
Abs	0.5	0.1	5	1	1	500
Mean	N/A	N/A	N/A	10	10	200

Note that the bending radius always converges to the lower end of the tolerance limit. This indicates that the bending radius should be kept at the minimum level. A contour plot for the maximum enveloping cable tension and actuator power for the optimal 2D-Betabot design

Table 5.4: The top 10 con…gurations and the associating performance index for 2D Betabot

	Con…guration						Performance					
	L_0	R_U	R_L	dHc	Y^{min}	d	w	h	F_c^{min}	T^{max}	W^{max}	E^{max}
	mm	mm	mm	mm	mm	mm	mm	mm	N	N	W	mm=mm
1	610	34	33	302	-669	285	1593	669	157	177	890	1.27
2	630	33	34	320	-680	270	1641	680	159	178	894	1.24
3	584	34	34	279	-654	274	1529	654	161	180	900	1.30
4	571	34	34	266	-644	305	1495	644	149	180	904	1.32
5	559	34	33	257	-638	315	1456	638	149	180	905	1.35
6	549	34	34	242	-627	292	1440	627	155	182	912	1.35

are shown in Figure 5-8 and Figure 5-9 respectively. Unlike the 2D-Deltabot, the maximum cable tension in the 2D-Betabot occurs in one location only. More importantly, there is no stationary point ($rT = 0$) in the workspace. As a result, if the maximum cable tension could have been identi…ed easily using conventional optimization process, and the result is would to still be the global maximum. This would be a major improvement in computational e¢ciency for the design optimization.

5.3 Prototype: 2D Deltabot

5.3.1 Prototype Design and Speci…cations

Due to the pass success in the development of a cable-based verision of Deltabot, it has been decided to implement the 2D Deltabot. While the design speci…cation is reasonable for most industrical applications, the production of a prototype does not is somewhat limited by the exsiting equipment, which includes three 0:47kW Kollmorgen servo motor and three Thompson Industries 12:1 right angle gear-reducer. The rated power for this drive system is 36N-m [7]. With the limited actuator power, none of the optimitial design con…guration could satisfy the design requirements. As a result, the maximum end-e¤ector speed is lowered to 2:0m=s and the optimial design con…guration is listed below:

L_0 = 150mm

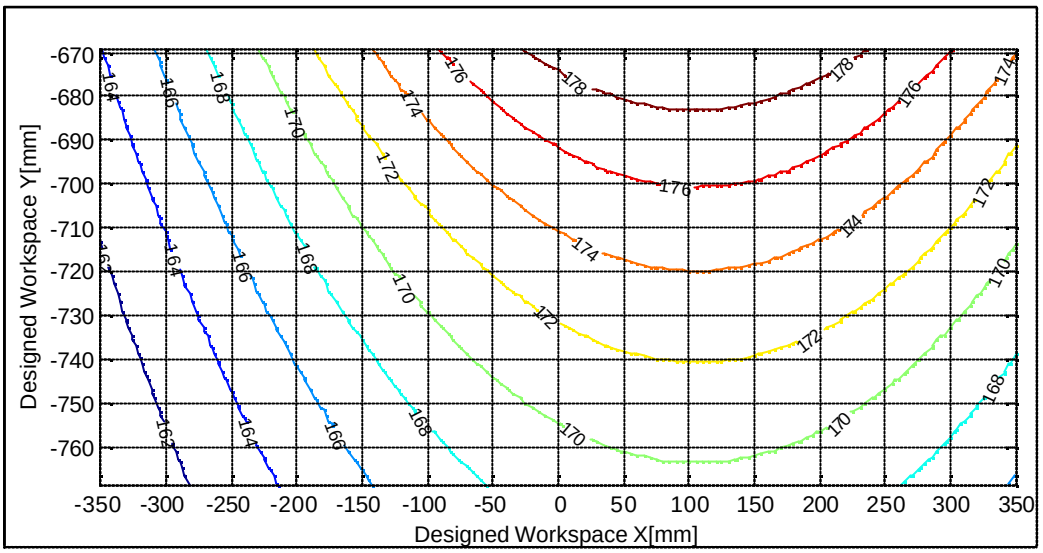

Figure 5-8: Maximum enveloping cable tension (occurs on the Side B) [N] for the optimal 2D-Betabot con…guration. Note Right this is Moment

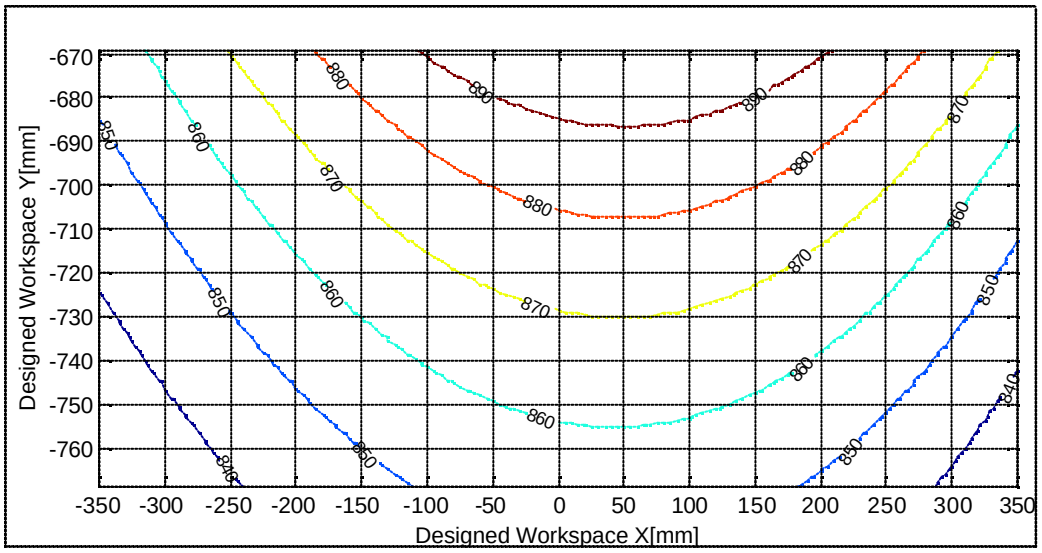

Figure 5-9: Maximum enveloping actuator power [W] of side B for the optimal 2D-Betabot con…guration.

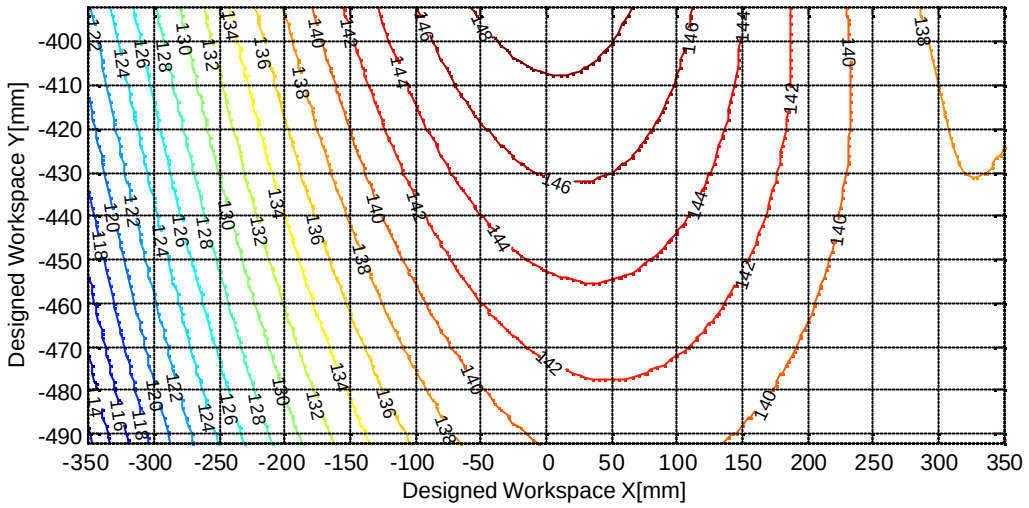

Figure 5-10: Maximum enveloping cable tension (occurs on the Side B) [N] for the 2D-Deltabot Prototype.

L_1 = 240mm

L_2 = 525mm

dH_c = 0mm

Y^{min} = 392mm

dP l = 75mm

With a reduction in the required maximum end-e¤ector speed, the maximum required actuator powers is reduced to 0:35kW and the maximum cable tension is reduced to 149N as illustrated in Figure 5-10 and Figure 5-11. Since the maximum end-e¤ector a¤ects both the dynamic cable force and the actuator speed, this is reasonable to have more than 50% reduction in actuator power when the required end-e¤ector speed is halved.

Another limiting factor in the prototype design is the limited amount of the available actuator torque. The prototype requires just under 36N m to operate at the rated speci…cation. Figure 5-12 shows the maximum actuator torque distribution of the prototype. A comparison between the maximum actuator torque (Figure 5-12) and the maximum cable tension (Figure 5-10) shows that the actuator torque is a¤ected more by the cable angle than the cable tension. More importantly, the maximum actutor torque ocurrs in a di¤erent location than

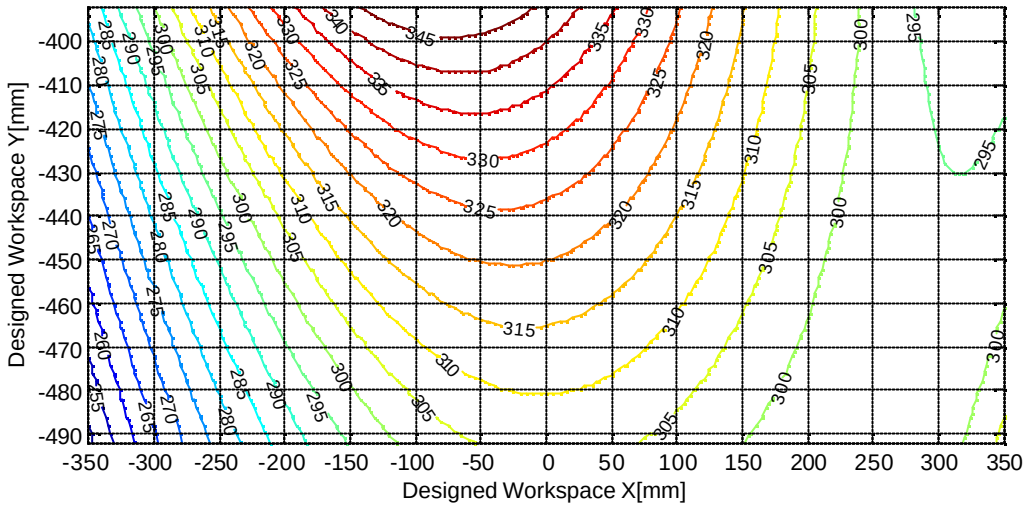

Figure 5-11: Maximum enveloping actuator power [W] of side B for the prototype 2D-Deltabot

the maximum torque. This there will be di¤erent limiting resource at di¤erent location of the workspace. Nonetheless, it is worthwhile to investigate the the region at which the manipulator can provide

5.3.2 Prototype Theroectical Perfomance analysis

Since the cylinder force is held constant throughout the workspace to ensure minimum tension at the rated performance, there are region in the workspace which may loses rigidity with it is driven beyond its designed speci…cation. A study in the minimum cable tension distribution would be necessary to determine the critical region where the manipulator loses ridigity. Figure 5-13 is a contour plot of the minimum cable tension in the robot workspace. Note that the minimum cable tension occurs in side A and its trend is virtually a mirror imagin from the maximum cable tension contour in Figure 5-10.

Since the minimum tension occurs in the upper left corner (when the e¤ective cable separating distance, $d \sin(\theta_A)$ is the smallest), it is not expected that the manipulator can perform any faster than it can at that location. Figure 5-14 shows the maximum velocity of the end-e¤ector under the worst case condition in the robot workspace. As expected from the previous observa-

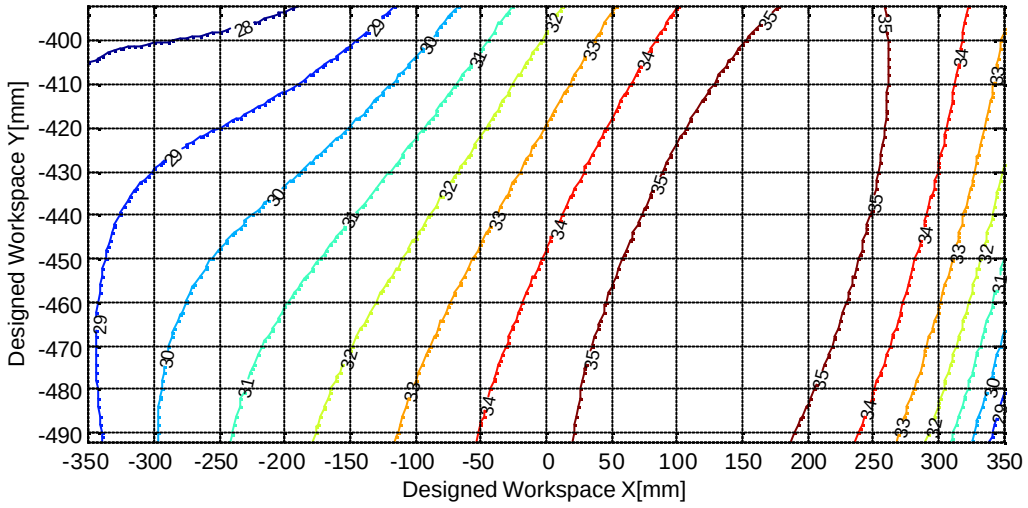

Figure 5-12: Maximum enveloping actuator torque [W] of side B for the prototype 2D-Deltabot

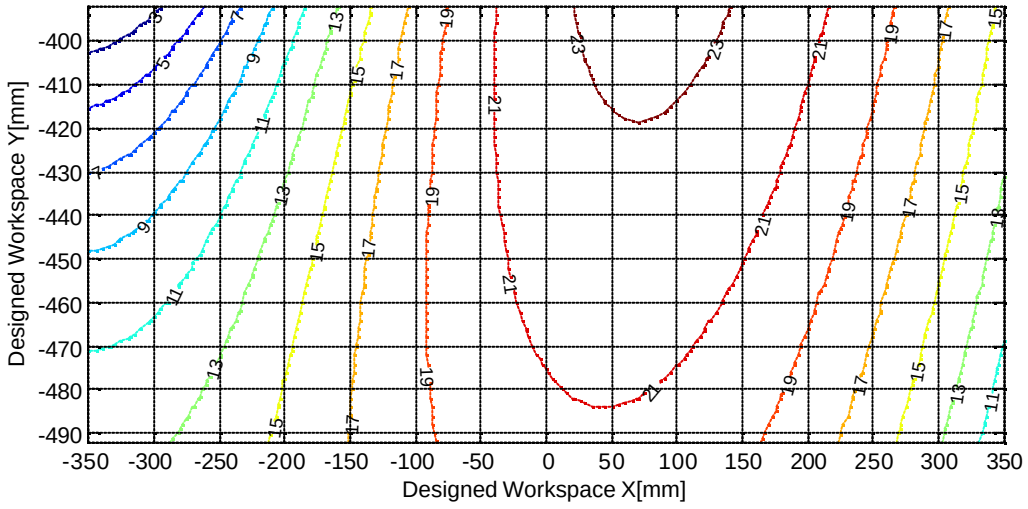

Figure 5-13: Minimum enveloping cable tension [T] of side A for the prototype 2D-Deltabot

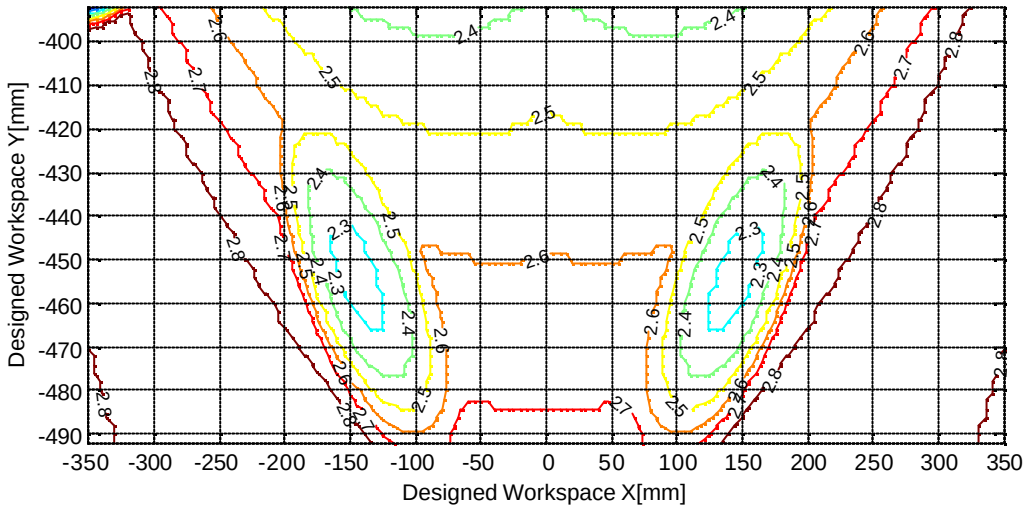

Figure 5-14: Maximum Velocity [m/s] of the prototype 2D-Deltabot

tion, the limiting speed of the prototype robot is signi…cantly slower in the upper left (opposite to the parallel cable joint) corner of the workspace, where the cable tension reaches minimum. Also, the limiting speed is also somewhat limited torwards the center of the workspace where the maximum actuator torque occurs

In the most optimial pick and place trajectory, the end-e¤ector should reach its maxmium speed at the center of the path. Therefore, it is reasonable to expected that the limiting speed is the maximum allawable speed near the upper center of the workspace. In the prototype design, it is approximately 2:5m=s. At this limiting speed, the robot can complete a 1:8m pick-and-place cycle (up 0:1m, across 0:7m, down 0:1m and goes back to the starting position) in 0:84s. This tranlsates to approximately 71 cycles / minutes.

Bibliography

[1] Machinery Handbook 25. Industrial Press Inc, 1996.

[2] Ming A. and Higuchi T. Study on multiple degree-of-freedom positioning mechanism using wires (part1). International Journal of Japan Society of Precision Engineering, 28(2):131–138, 1994.

[3] Mason F.-Sera...ni P. Andreatta, G. Advanced School on Stochastics in Combinatorial Optimization. World Scienti...c, Singapore, 1986 edition, 1986.

[4] Dennis J. Audet, C. A pattern search ...lter method for nonlinear programming without derivative. SIAM Journal on Optimization, v 14(n4):980–1010, 2004.

[5] Dekker R.-Khajepour A. Chan E. Behzadipour, S. Deltabot a new cable-based ultra high speed robotr. International Mechanical Engineering Congress and Expo, ASME, IMECE2003-41470, 2003.

[6] Rendon-Sanchez J. Cervantes-Sanchez, J. Simpli...ed approach for obtaining the workspace of a class of 2-dof planar parallel manipulators. Mechanism and Machine Theory, v34(7):1057–1073, 1999.

[7] E. Chan. The mechanical components of the ultra high speed pick and place robots. Technical report, 2002.

[8] R. Clavel. Device for the movement and positioning of an element in space. Technical report, 1990.

[9] J. Du¤y. Statics and Kinematics with Applications to Robots. Cambridge University Press, 1996 edition, 1996.

[10] Chetelat O. Ghorbel, F. A reduced model for constrained rigid bodies with application of parallel robots. Proc. of the IFAC Symposium on Robot Control, SYROCO, pages 57–62, Sept 1994.

[11] Whitehall S.G. Gough V.E. Univeral tyre test machine. Proceedings of 9th International Technical Conference F.I.S.I.T.A, pages 177–135, 1962.

[12] Zhanxian Li.-Meng Li. Chetwynd G. Cosselin M. Huang, T. Conceptual design and dimensional synthesis of a novel 2-dof translational parallel robot for pick and place operations. Journal of Mechanical Design, (7):449–455, 2004.

[13] Ingersoll. Octahedral machine tool frame. Technical report, 1995.

[14] Tsai L-W. Joshi, S. A comparison study of two 3-dof parallel manipulators: One with three and the other with four supporting legs. Proc. of IEEE International Conference on Robotics and Automation, pages 1288–1293, 1991.

[15] Choe W.-Tanak S. Kawamura, s. Development of an ultrahigh speed robot falcon using wire driven systems. pages 215–220, 1995.

[16] Behzadipour S.-Dekker R. Khajepour, A. Light weight parallel manipulators using active/passive cables. Technical report, 2002.

[17] Behzadipour S.-Dekker R. chan E. Khajepour, A. New cable-based ultra high speed robots, a review. International Conference on, Intelligent Manipulation and Grasping, IMG04, 2004.

[18] Tsai L-W. Kim, H. Design optimization of a cartesian parallel manipulator. Journal of Mechanical Design, transaction of the ASME, v125(n1):43–51, 2003.

[19] Tsai L-W. Kim, H. Kinematic synthesis of a spatial 3-rps parallel manipulator. Journal of Mechanical Design, transaction of the ASME, v125(n1):92–97, 2003.

[20] Sheridan T. Landsberger, S. A new design for parallel manipulators. Proceedings International Conference on Cybernetics and Society, pages 812–814, 1985.

[21] Torczon V. Lewis, M. A globally convergent augmented lagrangian pattern search algorithm for otpimization with general constraintes and simle bounds. SIAM Journal on Optimization, v 12(n4):1075–1089, 2002.

[22] Torczon V.-Trosset M. Lewis, M. Direct search methods: Then and now. Journal of Computational and Applied Mathematics, v124(n1-2):191–207, 2000.

[23] K. Mckinnon. Convergence of the nelder-mead simplex method to a nonstationary point. SIAM Journal on Optimization, v 9(n1):148–158, 1998.

[24] Gosselin C.-Mouly N. Merlet, J. Workspace of planar parallel manipulators. Mechanism and Machine Theory, v33(1-2):7–20, 1998.

[25] J-P. Merlet. Parallel Robots. Kluwer Academic Publishers, 1st edition, 2000.

[26] A.-Dauchez P. Pierrot F., Fournier. Towards a fully-parallel 6 dof robot for high-speed applications. Proc. of IEEE International Conference on Robotics and Automation, pages 1288–1293, 1991.

[27] D. Stewart. A platform with six degrees of freedom. Proceedings of the Institute of Mechanical Engineering, 180:371–386, 1965.

[28] Nishioka S.-Kimura T. Hattori M. Takamori T. Maeda K. Tadokoro, S. On fundamental design of wire con...gurations of wire-driven parallel manipulators with redundancy. 1:151–158, 1996.